Available online at www.sciencedirect.com
ScienceDirect
Comput. Methods Appl. Mech. Engrg. 196 (2007) 2596–2618
Computer methods in applied mechanics and engineering
www.elsevier.com/locate/cma

Hypersingular shape sensitivity boundary integral equation for crack identification under harmonic elastodynamic excitation

Guillermo Rus, Rafael Gallego *

Departamento de Mecánica de Estructuras, Politécnico de Fuentenueva, Universidad de Granada, Avda Fuentenueva s/n, 18071 Granada, Spain

Received 14 February 2006; received in revised form 4 December 2006; accepted 4 December 2006

Abstract

Model-based nondestructive testing (NDT) requires fast and accurate solutions of the response of the mechanical model including the defect as well as the sensitivity of this response to the variation of the parameters describing the defect. For modelling crack-type defects under dynamic conditions, like vibration analysis or ultrasonics, the boundary element method (BEM) is especially well suited, in particular due to the hypersingular formulation.

The present work presents the stress sensitivity boundary integral equation, δqBIE, and its use for the solution of the inverse problem when coupled to gradient-based minimization algorithms. The capability of solving numerically a NDT problem such as the location and characterization of cracks by measuring the dynamic response at an accessible boundary of the specimen is evaluated. For that, the accuracy and convergence of the sensitivity from the δqBIE is verified. Then, comprehensive convergence tests are made for the initial guess, the amount of supplied measurements, and simulated errors on measurements, geometry, elastic constants and frequency.

PACS: 43.40.L; 81.70

Keywords: Sensitivity; Identification inverse problem (IIP); Optimization algorithms; Quantitative non-destructive evaluation (QNDE); Boundary element method (BEM); Boundary integral equations (BIE); Hypersingular

1. Introduction

A direct problem can be stated as the calculation of the response (for instance, certain displacements u and tractions q) in a specific body defined by its geometry Ω, mechanical properties (k), physical model (operator L) and boundary conditions (some known values of u and q). In opposition to this, an *inverse problem* (IP) is one in which part of the information above is unknown. If a generic direct problem is defined as

$$L(k)u = q \quad \text{on } \Omega \tag{1}$$

different IPs can be stated depending on the nature of the unknown (see the classification by Kubo [1]). To find the missing information, additional data from the response has to be provided, besides the boundary conditions. This additional data u^{ex} or q^{ex} is obtained experimentally at some points of the domain or its boundary Γ.

This paper is aimed at the solution of the so called *identification inverse problem* (IIP), which is an IP in which the unknown is a part of the domain. This problem arises in many branches of science and engineering, but the interest of the authors is mainly the development of computerized non-destructive techniques, aimed at the detection of cracks inside a unreachable part of a mechanical or structural element.

An important limitation of the use of steady-state dynamic data for crack detection should be pointed out here. In this work, *no unilateral effects* or contact phenomena are considered in the crack for the following reasons:

* Corresponding author. Tel.: +34 958 24 89 55; fax: +34 958 249 959.
E-mail addresses: grus@ugr.es (G. Rus), gallego@ugr.es (R. Gallego).

0045-7825/$ - see front matter © 2007 Elsevier B.V. All rights reserved.
doi:10.1016/j.cma.2006.12.004

- The frequency domain based postprocessing is usually not applicable.
- The nonlinearities that appear in the model convert the optimization functions into non-differentiable ones, making the choice of optimization algorithm different from the classical gradient-based methods. The differentiation of the boundary integral equation becomes a nontrivial task.
- The solution of the nonlinear problem as well as the optimization algorithm, which would require bilevel techniques (a lower iteration level for the nonlinear system solution and an upper one for the optimization, which was studied thoroughly for the first time by Stavroulakis and Antes [2]), are dramatically more expensive computationally. This moves the balance towards noncontact testing.

The absence of contact marks off its field of applicability when the crack is initially open and kept so during the excitation. This is true as long as the small harmonic excitation load is applied on a preloaded structure where the crack is already open, which is the usual case, as the original load motivates the creation of the crack. This way, the specimen can be studied in service or working conditions, and the small harmonic excitation will not alter the null contact conditions of the crack.

A general IP can be written alternatively,

(1) as the solution of a set of implicit nonlinear equations called *observation equations*, that relate some properly chosen *design variables* P_h and the experimental data, v^{ex},

$$F(P_h) = v^{\text{ex}}$$

(2) or as an *optimization problem*, where the residual of the former set of equations is minimized,

$$\min_{P_h} \frac{1}{2}\|F(P_h) - v^{\text{ex}}\|^2.$$

In both cases, the most time-efficient solution algorithms use sensitivity information (gradient), which should be computed accurately and efficiently.

To perform this computation, besides the obvious but time-consuming finite differences approach, two analytical tools are available: direct differentiation method and adjoint state approach. The first one was used by Nishimura and Kobayashi [3], Meric [4], Aithal and Saigal [5], Mellings and Aliabadi [6], Lee and Kwak [7] or Rus and Gallego [8]. It is based on the direct differentiation of the equations with respect to the geometrical parameters which define the unknown flaw. Mukherjee et al. [9–11] develop the direct differentiation formulation for the indirect boundary contour method for 3D static elasticity, first for boundary points and then for internal points, and obtain moderately good convergence.

On the other hand Bonnet et al. [12], applied the adjoint state approach to the boundary integral equations to find the sensitivity to geometry variation of a crack in bidimensional elasticity and, later, in elastodynamics [13,14]. The same approach was used by Burczyński et al. [15] and compared to the direct differentiation.

The inverse problem of locating a cavity using elastodynamic measurements was solved using the adjoint state approach for the geometrical sensitivity and BFGS for minimization of the quadratic cost functional by Guzina et al. [16] for the case of 3D elastodynamics, attaining convergence for a single elipsoidal cavity.

In this paper, the *Stress Sensitivity Boundary Integral Equation* or *Variation Hypersingular Boundary Integral Equation* is derived from the standard BEM equation and used to supply the necessary geometrical gradient for the search algorithm used for solving a complete IIP. This method for determining the geometrical sensitivity is preferred above the adjoint state approach due to the much lower requirements on discretization density, which extends considerably the time of convergence. The goodness and capacity of convergence of the resulting algorithm is exhaustively checked. The *Sensitivity Hypersingular Boundary Integral Equation* provides the sensitivity of displacements and tractions in an harmonic elastodynamics state due to *changes in the geometry of an internal crack*. This equation is obtained by a series expansion and a linearization, following a procedure first proposed by Tanaka and Masuda [17] for potential problems, and Aithal and Saigal [5] for static elasticity. In these papers some important terms where missing and a first corrected formulation was presented for potential problems by Gallego and Suárez [18] in 1998 and by Rus and Gallego [19] in 2005. The final equation should be equivalent to that obtained by Bonnet [20] using material differentiation, but no attempt has been made yet to prove this.

2. Boundary integral equations

In a domain Ω bounded by Γ, the displacement integral equation (or *u*BIE, see [21]) can be written as

$$c_k^i(\mathbf{y})u_k(\mathbf{y}) + \int_\Gamma [q_k^i(\mathbf{x};\mathbf{y})u_k(\mathbf{x}) - u_k^i(\mathbf{x};\mathbf{y})q_k(\mathbf{x})]\,\mathrm{d}\Gamma(\mathbf{x}) = 0, \tag{2}$$

where $u_k(\mathbf{x})$, kth component of the displacement vector in the actual state at the *observation point* $\mathbf{x}$; $q_k(\mathbf{x})$, $=\sigma_{jk}(\mathbf{x})n_j(\mathbf{x})$ traction in the actual state at point $\mathbf{x}$. $\sigma_{jk}(\mathbf{x})$ is the stress tensor and n_j the outward normal; $u_k^i(\mathbf{x};\mathbf{y})$, kth component of the displacement vector at the observation point $\mathbf{x}$ due to a point load applied in direction i at the *collocation point* $\mathbf{y}$ (fundamental solution); $q_k^i(\mathbf{x};\mathbf{y})$, $=\sigma_{lk}^i(\mathbf{x};\mathbf{y})n_l(\mathbf{x})$ traction of the fundamental solution; c_k^i, free term whose value depends on the position of the collocation point. Thus, $c_k^i(\mathbf{y}) = \delta_k^i$ (Kroenecker delta) if $\mathbf{y} \in \Omega$; $c_k^i(\mathbf{y})$ depends on the geometry of the boundary at $\mathbf{y}$ if

$\mathbf{y} \in \Gamma$, and is such that $c_k^i(\mathbf{y}) = 1/2\delta_k^i$ when the boundary is smooth (continuous normal) at $\mathbf{y}$; $c_k^i(\mathbf{y}) = 0$ otherwise.

The integral is understood in the Cauchy Principal Value (CPV) sense. The variables in this equation are complex numbers that represent the amplitude (modulus) and phase (argument) of the harmonic real ones.

The fundamental solution for two-dimensional harmonic elastodynamics is given by

$$u_k^i = \frac{1}{2\pi\mu}[\psi\delta_{ik} - \chi r_{,i} r_{,k}], \tag{3}$$

$$\begin{aligned} q_k^i = \frac{1}{2\pi}\Bigg[& \left(\phi' - \frac{\chi}{r}\right)(\delta_{ik} r_{,j} n_j + r_{,i} r_{,k}) \\ & - \frac{2}{r}\chi(n_k r_{,i} - 2 r_{,k} r_{,i} r_{,j} n_j) - 2\chi' r_{,i} r_{,k} r_{,j} n_j \\ & + \left(\frac{c_p^2}{c_s^2} - 2\right)\left(\phi' - \chi' - \frac{\chi}{r}\right) r_{,i} n_k \Bigg], \end{aligned} \tag{4}$$

where $r_i = x_i - y_i$, $r = |\mathbf{r}|$; $r_{,i} = \frac{\partial r}{\partial x_i}$. ψ and χ are functions of the position r and excitation frequency ω, given by the expressions

$$\psi = K_0(k_s r) + \frac{1}{k_s r}\left[K_1(k_s r) - \frac{c_s}{c_p} K_1(k_p r)\right], \tag{5}$$

$$\chi = K_2(k_s r) - \frac{c_s^2}{c_p^2} K_2(k_p r), \tag{6}$$

where, $k_\alpha = \frac{i\omega}{c_\alpha}$, and c_p and c_s are the P-waves and S-waves propagation speeds, respectively; $K_n(z)$ is the modified Bessel function of order n.

The equivalent integral equation for the stresses on the boundary can be computed by application of Hooke's law to the previous equation,

$$q_i(\mathbf{y}) = \{\lambda\delta_{ij} u_{m,m}(\mathbf{y}) + \mu(u_{i,j}(\mathbf{y}) + u_{j,i}(\mathbf{y}))\} n_j(\mathbf{y}) \tag{7}$$

yielding,

$$c_k^i(\mathbf{y}) q_k(\mathbf{y}) + \int_\Gamma [d_k^i(\mathbf{x};\mathbf{y}) q_k(\mathbf{x}) - s_k^i(\mathbf{x};\mathbf{y}) u_k(\mathbf{x})]\, d\Gamma(\mathbf{x}) = 0. \tag{8}$$

The equation in this form is only valid for internal collocation points ($\mathbf{y} \in \Omega\Gamma$, $c_k^i = \delta_k^i$) or on a smooth boundary ($c_k^i(\mathbf{y}) = 1/2\delta_k^i$). In this last case the integral can be understood in the sense of the Cauchy principal value or Hadamard finite part (see [22–24]).

The kernels in this integral equation (qBIE for short) are obtained from the ones in Eq. (2) using Hooke's law,

$$\begin{aligned} & d_k^i(\mathbf{x};\mathbf{y}) = d_{kj}^i(\mathbf{x};\mathbf{y}) n_j(\mathbf{y}), \\ & d_{kj}^i(\mathbf{x};\mathbf{y}) = \lambda\delta_{ij} u_{k,m}^m(\mathbf{x};\mathbf{y}) + \mu(u_{k,j}^i(\mathbf{x};\mathbf{y}) + u_{k,i}^j(\mathbf{x};\mathbf{y})), \\ & s_k^i(\mathbf{x};\mathbf{y}) = s_{jkl}^i(\mathbf{x};\mathbf{y}) n_j(\mathbf{y}) n_l(\mathbf{x}), \\ & s_{jkl}^i(\mathbf{x};\mathbf{y}) = \lambda\delta_{ij}\sigma_{lk,m}^m(\mathbf{x};\mathbf{y}) + \mu(\sigma_{lk,j}^i(\mathbf{x};\mathbf{y}) + \sigma_{lk,i}^j(\mathbf{x};\mathbf{y})), \end{aligned} \tag{9}$$

where the derivatives are performed with respect to the coordinates of $\mathbf{x}$, and the fact that $\partial/\partial x_m = -\partial/\partial y_m$ for the kernels since they are functions of the distance $\mathbf{r} = \mathbf{x} - \mathbf{y}$, has been taken into account.

3. Derivation of the δqBIE

Assume a domain Ω bounded by a boundary Γ under essential and natural boundary conditions. This problem will be termed *reference problem* or RP and its solution is readily computed by the standard BEM. Consider now a modified domain $\widetilde{\Omega}$ due to a slight alteration of its boundary or part of it, to $\widetilde{\Gamma}$. The modified boundary can be just an internal crack within Ω. This second problem is termed *perturbed problem* or PP. For both problems the material properties and boundary conditions are the same.

The variation of the geometry will be given by a vector $\delta\mathbf{x}$ such that,

$$\tilde{\mathbf{x}} = \mathbf{x} + \delta\mathbf{x}(\mathbf{x}). \tag{10}$$

Note that $\delta\mathbf{x}$ is defined at every $\mathbf{x} \in \Omega$ and not only on the boundary. The solutions of the reference and perturbed problems will be different, due to the change in the geometry,

$$\begin{aligned} \tilde{u}_i(\tilde{\mathbf{x}}) &= u_i(\mathbf{x}) + \delta u_i(\mathbf{x}), \\ \tilde{q}_i(\tilde{\mathbf{x}}) &= q_i(\mathbf{x}) + \delta q_i(\mathbf{x}), \end{aligned} \tag{11}$$

where the tilde is applied to any variable at the PP and $\delta\mathbf{u}$ and $\delta\mathbf{q}$ represents the *shape variation* or shape sensitivity of the displacements and tractions, respectively. Observe that where essential boundary conditions are given $\delta u_i(\mathbf{x}) = 0$, whereas where the conditions are natural $\delta q_i(\mathbf{x}) = 0$.

The goal is to obtain a boundary only integral equation which relates the sensitivities of boundary displacements and tractions to the variation of the geometry.

The procedure to obtain this boundary integral equation follows these steps:

(1) The stress integral equation for an interior point is written for both the RP and PP.
(2) The integrals and integrands in the integral equation for the PP are expanded to first order, in terms of the geometry variation.
(3) Subtracting the integral equation for the RP to the linearized integral equation for the PP, the stress sensitivity integral equation is obtained for an interior point.
(4) The resulting integral equation is taken to the boundary, taking care of the order of the singular kernels and the required continuity of the variables.

The procedure is summarized in Fig. 1.

The ensuing equation will be termed *Stress Sensitivity Boundary Integral Equation* or δqBIE. Its numerical solution is tackled using standard Boundary Element Techniques, plus some non-standard approaches to discretize the variation of the geometry.

After computing the shape sensitivities of displacements and tractions on the boundary, the variation of any functional of the variables,

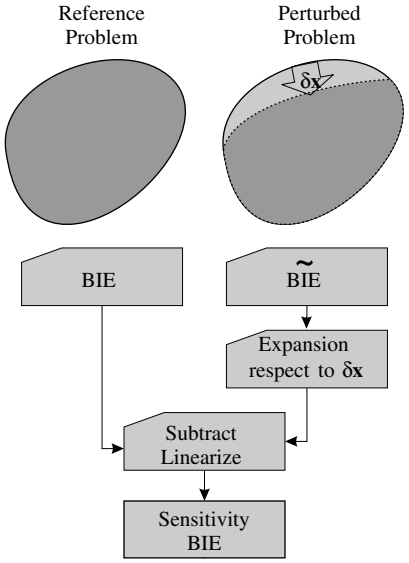

Fig. 1. Procedure to obtain the variation integral equation.

$$J(\Gamma) = \int_{\Gamma_q} \varphi_u(\mathbf{u})\,\mathrm{d}\Gamma + \int_{\Gamma_u} \varphi_q(\mathbf{q})\,\mathrm{d}\Gamma + \int_{\Gamma_f} \psi(\mathbf{x})\,\mathrm{d}\Gamma \tag{12}$$

can be computed using the chain rule,

$$\delta J(\Gamma) = \int_{\Gamma_q} \frac{\partial \varphi_u}{\partial \mathbf{u}}\delta\mathbf{u}\,\mathrm{d}\Gamma + \int_{\Gamma_u} \frac{\partial \varphi_q}{\partial \mathbf{q}}\delta\mathbf{q}\,\mathrm{d}\Gamma + \int_{\Gamma_f} \frac{\partial \psi}{\partial \mathbf{x}}\delta\mathbf{x}\,\mathrm{d}\Gamma \tag{13}$$

assuming that Γ_q, Γ_u, and Γ_f belongs to an unperturbed part of the boundary, which is the case in the identification inverse problems.

The functional may include domain terms since the sensitivities at internal points can be computed as a postprocessing step using the corresponding integral equation.

4. Variation of the boundary differential and the normal vector

As a first step for developing the δqBIE, the variation of some geometrical quantities that arise is considered in this section.

The variation of the normal and the boundary differential are defined by

$$\begin{aligned} \tilde{\mathbf{n}} &= \mathbf{n} + \delta\mathbf{n} + \text{h.o.t.},\\ \mathrm{d}\tilde{\Gamma} &= (1+\delta J)\,\mathrm{d}\Gamma + \text{h.o.t.}, \end{aligned} \tag{14}$$

where h.o.t. stands for *higher order terms*.

4.1. Variation of the boundary differential

In Fig. 2 the relationship between the boundary differential at the reference and perturbed domain is shown.

At a boundary point $\boldsymbol{\xi} \in \Gamma$ the boundary differential is defined by

$$\mathrm{d}\Gamma^2 = \mathrm{d}\xi_i\,\mathrm{d}\xi_i. \tag{15}$$

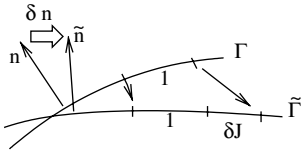

Fig. 2. Variation of the boundary differential.

After the perturbation $\tilde{\boldsymbol{\xi}} = \boldsymbol{\xi} + \delta\boldsymbol{\xi}$, and therefore the differential is given by

$$\mathrm{d}\tilde{\Gamma}^2 = (\mathrm{d}\xi_i + \mathrm{d}\delta\xi_i)(\mathrm{d}\xi_i + \mathrm{d}\delta\xi_i). \tag{16}$$

Expanding the product and neglecting terms higher than linear,

$$\mathrm{d}\tilde{\Gamma}^2 \simeq \mathrm{d}\Gamma^2 + 2\mathrm{d}\xi_i\,\mathrm{d}\delta\xi_i \tag{17}$$

and then,

$$\mathrm{d}\tilde{\Gamma}^2 \simeq \mathrm{d}\Gamma^2 + 2\mathrm{d}\xi_i\delta\xi_{i,j}\,\mathrm{d}\xi_j. \tag{18}$$

Taking the square root and neglecting again higher order terms,

$$\mathrm{d}\tilde{\Gamma} \simeq \mathrm{d}\Gamma(1 + \delta\xi_{i,j}t_i t_j), \tag{19}$$

where

$$t_i = \frac{\mathrm{d}\xi_i}{\mathrm{d}\Gamma} \tag{20}$$

are the components of the tangent vector at $\boldsymbol{\xi}$. Therefore,

$$\delta J = \delta\xi_{i,j}t_i t_j. \tag{21}$$

4.2. Variation of the normal vector

In Fig. 3 the variation of the normal at a boundary point is represented.

To obtain the variation of the normal vector is more convenient to compute first the variation of the tangent vector. From Eq. (20), the components of the tangent vector after perturbation are

$$\tilde{t}_i = \frac{\mathrm{d}\tilde{\xi}_i}{\mathrm{d}\tilde{\Gamma}} = \frac{\mathrm{d}\xi_i + \mathrm{d}\delta\xi_i}{\mathrm{d}\Gamma(1+\delta J)}. \tag{22}$$

Neglecting terms higher than linear,

$$\tilde{t}_i = t_i - t_i\delta J + \delta\xi_{i,j}t_j. \tag{23}$$

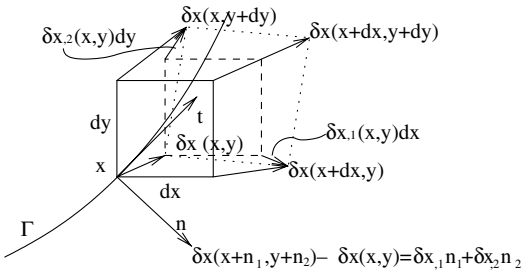

Fig. 3. Differential geometrical in the vicinity of ξ.

Since the tangent vector has unit modulus, the second term can be neglected,

$$\tilde{t}_i = t_i + \delta\xi_{i,j}t_j. \tag{24}$$

Now, the normal is perpendicular to the tangent vector, then

$$\tilde{n}_i = n_i + \epsilon_{ik}\delta\xi_{k,j}t_j, \tag{25}$$

where ϵ_{ik} is the permutation tensor. But, to maintain the unit modulus, only the component of the variation perpendicular to the normal is kept,

$$\tilde{n}_i = n_i + t_i t_l \epsilon_{lk}\delta\xi_{k,j}t_j. \tag{26}$$

Therefore,

$$\delta\mathbf{n} = \epsilon_{ij}\delta\xi_{j,k}t_i t_k \mathbf{t}. \tag{27}$$

5. Variation of the integral equation

Consider the qBIE for an collocation point inside the perturbed domain,

$$\tilde{q}_i(\tilde{\mathbf{y}}) + \int_{\tilde{\Gamma}}[d^i_k(\tilde{\mathbf{x}};\tilde{\mathbf{y}})\tilde{q}_k(\tilde{\mathbf{x}}) - s^i_k(\tilde{\mathbf{x}};\tilde{\mathbf{y}})\tilde{u}_k(\tilde{\mathbf{x}})]\,\mathrm{d}\tilde{\Gamma}(\tilde{\mathbf{x}}) = 0. \tag{28}$$

The first step is to expand all terms in the above equation about the reference configuration considering a small perturbation of the geometry. The expansion of the unknown displacements and tractions are given by the definition of the sensitivity in Eq. (11).

The two point kernels have to be expanded taking into account that both the collocation point $\mathbf{y}$ and the observation point $\mathbf{x}$ are perturbed. Moreover, d^i_k depends on the normal at the observation point $\mathbf{n}(\mathbf{x})$ while s^i_k depends on the normal at both the observation and collocation points, $\mathbf{n}(\mathbf{x})$ and $\mathbf{n}(\mathbf{y})$ (see Eq. (31)).

Therefore,

$$\begin{aligned} d^i_k(\tilde{\mathbf{x}};\tilde{\mathbf{y}}) &= d^i_{kj}(\tilde{\mathbf{x}};\tilde{\mathbf{y}})\tilde{n}_j(\tilde{\mathbf{y}}) \\ &= (d^i_{kj}(\mathbf{x};\mathbf{y}) + \delta d^i_{kj}(\mathbf{x};\mathbf{y}))(n_j(\mathbf{y}) + \delta n_j(\mathbf{y})) + \text{h.o.t.}, \\ s^i_k(\tilde{\mathbf{x}};\tilde{\mathbf{y}}) &= s^i_{jkl}(\tilde{\mathbf{x}};\tilde{\mathbf{y}})\tilde{n}_j(\tilde{\mathbf{y}})\tilde{n}_l(\tilde{\mathbf{x}}) \\ &= (s^i_{jkl}(\mathbf{x};\mathbf{y}) + \delta s^i_{jkl}(\mathbf{x};\mathbf{y}))(n_j(\mathbf{y}) + \delta n_j(\mathbf{y})) \\ &\quad \times (n_l(\mathbf{x}) + \delta n_l(\mathbf{x})) + \text{h.o.t.} \end{aligned} \tag{29}$$

The perturbations of d^i_{kj} and s^i_{jkl} are simply computed by Taylor expansion,

$$\begin{aligned} \delta d^i_{kj}(\mathbf{x};\mathbf{y}) &= d^i_{kj,m}(\mathbf{x};\mathbf{y})\delta r_m, \\ \delta s^i_{jkl}(\mathbf{x};\mathbf{y}) &= s^i_{jkl,m}(\mathbf{x};\mathbf{y})\delta r_m, \end{aligned} \tag{30}$$

where $\delta r_m = \delta x_m - \delta y_m$ arises form the fact that the kernels depend on $\mathbf{x}-\mathbf{y}$ but not on $\mathbf{y}$ nor $\mathbf{x}$ independently.

From the above expansions, and neglecting terms of order higher than linear, the following expansions are obtained:

$$\begin{aligned} d^i_k(\tilde{\mathbf{x}};\tilde{\mathbf{y}}) &= d^i_k(\mathbf{x};\mathbf{y}) + d^i_{kj,m}(\mathbf{x};\mathbf{y})n_j(\mathbf{y})\delta r_m \\ &\quad + d^i_{kj}(\mathbf{x};\mathbf{y})\delta n_j + \text{h.o.t.}, \\ s^i_k(\tilde{\mathbf{x}};\tilde{\mathbf{y}}) &= s^i_k(\mathbf{x};\mathbf{y}) + s^i_{jkl}(\mathbf{x};\mathbf{y})n_j(\mathbf{y})\delta n_l(\mathbf{x}) \\ &\quad + s^i_{jkl}(\mathbf{x};\mathbf{y})\delta n_j(\mathbf{y})n_l(\mathbf{x}) \\ &\quad + s^i_{jkl,m}(\mathbf{x};\mathbf{y})\delta r_m n_j(\mathbf{y})n_l(\mathbf{x}) + \text{h.o.t.} \end{aligned} \tag{31}$$

Collecting the expansions of the kernels, variables and boundary differential equations (31), (21), (27)), substituting in the integral equation (28) and subtracting the same equation for the reference configuration, the sensitivity stress integral equation at an interior point is obtained,

$$\begin{aligned} &\delta^i_k\delta q_k(\mathbf{y}) + \int_\Gamma [d^i_k(\mathbf{x};\mathbf{y})\delta q_k(\mathbf{x}) - s^i_k(\mathbf{x};\mathbf{y})\delta u_k(\mathbf{x})]\,\mathrm{d}\Gamma(\mathbf{x}) \\ &= \int_\Gamma [(s^i_{jkl}(\mathbf{x};\mathbf{y})n_j(\mathbf{y})n_l(\mathbf{x})u_k(\mathbf{x}) \\ &\quad - d^i_{jk}(\mathbf{x};\mathbf{y})n_j(\mathbf{y})q_k(\mathbf{x}))\delta J(\mathbf{x}) \\ &\quad + (s^i_{jkl}(\mathbf{x};\mathbf{y})n_l(\mathbf{x})u_k(\mathbf{x}) - d^i_{jk}(\mathbf{x};\mathbf{y})q_k(\mathbf{x}))\delta n_j(\mathbf{y}) \\ &\quad + (s^i_{jkl,m}(\mathbf{x};\mathbf{y})n_l(\mathbf{x})n_j(\mathbf{y})u_k(\mathbf{x}) \\ &\quad - d^i_{jk,m}(\mathbf{x};\mathbf{y})n_j(\mathbf{y})q_k(\mathbf{x}))\delta r_m \\ &\quad + s^i_{jkl}(\mathbf{x};\mathbf{y})n_j(\mathbf{y})u_k\delta n_l(\mathbf{x})]\,\mathrm{d}\Gamma(\mathbf{x}). \end{aligned} \tag{32}$$

Note that, assuming that the reference problem is solved, and given a geometrical perturbation, the above equation relates the stress vector at any internal point to the displacements and tractions on the boundary. If this equation is written for $\mathbf{y}\in\Gamma$, the ensuing equation provides a boundary only formula to compute sensitivities on the boundary to changes in the geometry of the domain.

6. Limit to the boundary

Eq. (32) cannot be directly set for $\mathbf{y}\in\Gamma$ since the kernels would be singular, or hypersingular, using a usual term in Boundary Integral literature. A standard procedure is used to perform the limit, perturbing the boundary around the collocation point as shown in Fig. 4 and then evaluating the limit of the ensuing integrals as $\varepsilon\to 0$.

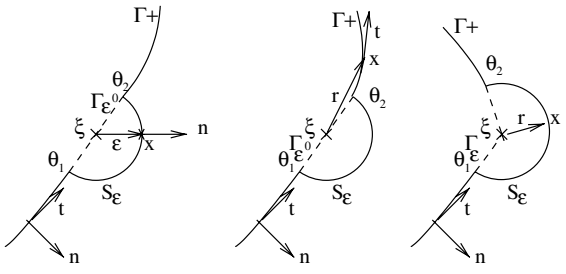

Fig. 4. Artifice for limiting process. Left: $\mathbf{x}\in\Gamma_\varepsilon$. Middle: $\mathbf{x}\in\Gamma_+$ after Γ_ε. Right: case of a non-smooth boundary.

Prior to the limiting process is therefore to asses the order of singularity of all the kernels and the corresponding continuity requirements for the variables.

6.1. Kernels' singularity and continuity requirements

The kernels of the standard qBIE, d^i_k, s^i_k, appear in the left hand side of Eq. (32), which are singular and hypersingular, respectively, that is

$$\begin{aligned} d^i_{kj}(\mathbf{x};\mathbf{y}) &= \mathrm{O}(r^{-1}),\\ s^i_{jkl}(\mathbf{x};\mathbf{y}) &= \mathrm{O}(r^{-2}), \end{aligned} \tag{33}$$

where $r = |\mathbf{x}-\mathbf{y}|$.

On the right hand side, the same kernels appear, plus their derivatives

$$\begin{aligned} d^i_{kj,m}(\mathbf{x};\mathbf{y}) &= \mathrm{O}(r^{-2}),\\ s^i_{jkl,m}(\mathbf{x};\mathbf{y}) &= \mathrm{O}(r^{-3}). \end{aligned} \tag{34}$$

Apparently, the sensitivity equation is one order more singular that the reference equation qBIE. However, observe that these two last kernels are multiplied by $\delta r_m = \delta x_m - \delta y_m$, so, if $\delta r_m \in C^\circ$,

$$\begin{aligned} d^i_{kj,m}(\mathbf{x};\mathbf{y})\delta r_m &= \mathrm{O}(r^{-1}),\\ s^i_{jkl,m}(\mathbf{x};\mathbf{y})\delta r_m &= \mathrm{O}(r^{-2}) \end{aligned} \tag{35}$$

and therefore, there is no increase in the singularity order. Actually δr_m should be $C^{1,\alpha}$ as shown later.

The singularity order of kernels demands a corresponding continuity order on the variables which multiplied them, in order to yield regular expressions. Thus,

$$\begin{aligned} &d^i_{jk}(\mathbf{x};\boldsymbol{\xi})\delta q_k(\mathbf{x}) \to \delta q_k(\mathbf{x}) = \delta q_k(\boldsymbol{\xi}) + \text{h.o.t.},\\ &s^i_{jkl}(\mathbf{x};\boldsymbol{\xi})\delta u_k(\mathbf{x}) \to \delta u_k(\mathbf{x}) = \delta u_k(\boldsymbol{\xi}) + \delta u_{k,m}(x_m-\xi_m) + \text{h.o.t.},\\ &d^i_{jk}(\mathbf{x};\boldsymbol{\xi})q_k(\mathbf{x}) \to q_k(\mathbf{x}) = q_k(\boldsymbol{\xi}) + \text{h.o.t.},\\ &s^i_{jkl}(\mathbf{x};\boldsymbol{\xi})u_k(\mathbf{x}) \to u_k(\mathbf{x}) = u_k(\boldsymbol{\xi}) + u_{k,m}(\boldsymbol{\xi})(x_m-\xi_m) + \text{h.o.t.} \end{aligned} \tag{36}$$

and same requirements from the rest of the integrals. Besides, $\delta x_{l,m}$ has to be continuous, i.e., $\delta x_m \in C^{1,\alpha}$.

Table 1 summarizes the continuity requirements for the variables, in order to regularize the integrals and perform the limit to the boundary.

These conditions have to be met by the boundary approximation used to solve numerically the ensuing BIE.

Table 1
Conditions of derivability of each variable

Variable	Continuity for δqBIE
u_k	$C^{1,\alpha}$
q_k	$C^{0,\alpha}$
δx_k	$C^{1,\alpha}$
δu_k	$C^{1,\alpha}$
δq_k	$C^{1,\alpha}$

6.2. Boundary decomposition and free terms

The integrals of any integrand F along the augmented boundary are decomposed in two parts,

$$\int_\Gamma F\,\mathrm{d}\Gamma = \int_{\Gamma-\Gamma_\varepsilon} F\,\mathrm{d}\Gamma + \int_{S_\varepsilon} F\,\mathrm{d}\Gamma. \tag{37}$$

For singular kernels ($\mathrm{O}(r^{-1})$) the first integral is the Cauchy Principal Value of the original integral, while the second one vanishes or lead to a finite free term.

For hypersingular kernels ($\mathrm{O}(r^{-2})$) both integrals leads to infinite terms, but these vanish, leading to the Hadamard finite value of the original integral, while, in addition, the second integral, along S_ε leads to finite free terms.

6.3. Free terms

Only the case of a smooth boundary point will be considered, since as in the original qBIE, standard interpolation demands that collocation points are placed inside the elements, where the boundary is smooth.

The free terms stem from the analytically calculable integrals along S_ε. At smooth boundary points, the integration can be done between $\delta\theta_1 = 0$ and $\delta\theta_2 = \pi$, without loss of generality.

On the boundary S_ε, the following identities hold:

$$\begin{aligned} &r = \varepsilon,\\ &r_k = \varepsilon n_k,\\ &\mathbf{n} = (\cos\theta, \sin\theta),\\ &\mathbf{t} = (-\sin\theta, \cos\theta),\\ &\mathrm{d}\Gamma = \varepsilon\,\mathrm{d}\theta, \end{aligned} \tag{38}$$

thus, a careful process finally yields the following expression, for which the details are provided in Appendix A,

$$\begin{aligned} &\int_{S_\varepsilon} [d^i_k(\mathbf{x};\mathbf{y})\delta q_k(\mathbf{x}) - s^i_k(\mathbf{x};\mathbf{y})\delta u_k(\mathbf{x})]\,\mathrm{d}\Gamma(\mathbf{x})\\ &\quad - \int_{S_\varepsilon} [(s^i_{jkl}(\mathbf{x};\mathbf{y})n_j(\mathbf{y})n_l(\mathbf{x})u_k(\mathbf{x})\\ &\quad - d^i_{jk}(\mathbf{x};\mathbf{y})n_j(\mathbf{y})q_k(\mathbf{x}))\delta J(\mathbf{x}) + (s^i_{jkl}(\mathbf{x};\mathbf{y})n_l(\mathbf{x})u_k(\mathbf{x})\\ &\quad - d^i_{jk}(\mathbf{x};\mathbf{y})q_k(\mathbf{x}))\delta n_j(\mathbf{y})\\ &\quad + (s^i_{jkl,m}(\mathbf{x};\mathbf{y})n_l(\mathbf{x})n_j(\mathbf{y})u_k(\mathbf{x})\\ &\quad - d^i_{jk,m}(\mathbf{x};\mathbf{y})n_j(\mathbf{y})q_k(\mathbf{x}))\delta r_m\\ &\quad + s^i_{jkl}(\mathbf{x};\mathbf{y})n_j(\mathbf{y})u_k\delta n_l(\mathbf{x})]\,\mathrm{d}\Gamma(\mathbf{x})\\ &\quad = -\frac{1}{2}\delta q_i + F_i \lim_{\varepsilon\to 0}\frac{1}{\varepsilon}. \end{aligned} \tag{39}$$

As mentioned above, the infinite free term cancels an equal expression from the integral along $\Gamma - \Gamma_\varepsilon$ leading to the Hadamard finite part of the original integral.

Collecting these results, the *Stress Sensitivity Boundary Integral Equation* (or δqBIE) at a smooth boundary point is finally obtained,

$$\frac{1}{2}\delta q_i \int_\Gamma [d^i_k(\mathbf{x};\mathbf{y})\delta q_k(\mathbf{x}) - s^i_k(\mathbf{x};\mathbf{y})\delta u_k(\mathbf{x})]\,\mathrm{d}\Gamma(\mathbf{x}) = \int_\Gamma [(s^i_{jkl}(\mathbf{x};\mathbf{y})n_j(\mathbf{y})n_l(\mathbf{x})u_k(\mathbf{x}) - d^i_{jk}(\mathbf{x};\mathbf{y})n_j(\mathbf{y})q_k(\mathbf{x}))\delta J(\mathbf{x}) + (s^i_{jkl}(\mathbf{x};\mathbf{y})n_l(\mathbf{x})u_k(\mathbf{x}) - d^i_{jk}(\mathbf{x};\mathbf{y})q_k(\mathbf{x}))\delta n_j(\mathbf{y}) + (s^i_{jkl,m}(\mathbf{x};\mathbf{y})n_l(\mathbf{x})n_j(\mathbf{y})u_k(\mathbf{x}) - d^i_{jk,m}(\mathbf{x};\mathbf{y})n_j(\mathbf{y})q_k(\mathbf{x}))\delta r_m + s^i_{jkl}(\mathbf{x};\mathbf{y})n_j(\mathbf{y})u_k\delta n_l(\mathbf{x})]\,\mathrm{d}\Gamma(\mathbf{x}), \tag{40}$$

where the integrals are understood in the sense of CPV or HFP of the original ones. This integral equation relates the variation ($\delta\mathbf{x}$ and δr_m) of a domain point $\mathbf{x}$ with the variation of displacements and tractions (δu_k and δq_k) at the boundary points, and the variation of the geometry of the boundary (δn_j and δS).

7. Numerical solution of the stress sensitivity BIE

Standard boundary element techniques are employed to solve the δqBIE. The boundary is divided into a number of elements, and within each one the geometry, displacements, tractions and their variations are interpolated quadratically, where ϕ_n are standard quadratic base functions,

$$\mathbf{x} = \sum_{n=1}^{3}\phi_n\mathbf{x}^n, \quad \mathbf{u} = \sum_{n=1}^{3}\phi_n\mathbf{u}^n, \quad \mathbf{q} = \sum_{n=1}^{3}\phi_n\mathbf{q}^n,$$

$$\delta\mathbf{u} = \sum_{n=1}^{3}\phi_n\mathbf{u}^n, \quad \delta\mathbf{q} = \sum_{n=1}^{3}\phi_n\mathbf{q}^n,$$

where ϕ_n are standard quadratic functions. However, due to the continuity requirements at the collocation points, non conforming elements will be employed, instead of isoparametric ones. Besides, when dealing with crack problems, non-conforming quarter point elements will be used.

For the variation of the geometry $\delta\mathbf{x}$ a different approach is followed,

$$\delta\mathbf{x} = \Theta_{ih}(\mathbf{x})\delta P_h, \tag{41}$$

where δP_h represents a finite number of variables which parameterize *the variation of the geometry*. Note that no parameterization of the geometry of the boundary is needed, but only of its variation. This point is detailed in the next section.

8. Parameterization of the variation of a crack shape

For cavities and inclusion identification, the *virtual deformation field* has been proposed [25] but this approach has limited interest when dealing with cracks, since it does not have enough flexibility to transform straight initial geometry to curved ones.

An advantage of the virtual deformation approach is that $\delta\mathbf{x}_k$ is defined not only on the boundary but in its vicinity as well, allowing the computation of the derivatives $\delta\mathbf{x}_{k,m}$. Nevertheless, any parameterization of the boundary can be extended to point in domain in the normal to the boundary point, transforming the derivatives to surface gradients, see [26].

Another issue related to the discretization of the variation of the geometry is its relationship to the discretization of the geometry itself. There are two main ways to use the parametrization inside the discretized sensitivity boundary integral equation:

- $\delta\mathbf{x} = \delta\mathbf{x}(\mathbf{x})$, which means that at an integration point x, the value of the matrix $\delta\mathbf{x}$ is computed using Eq. (41) using the coordinates of $\mathbf{x}$. This is the closest to the analytical definition.
- $\delta\mathbf{x} = \sum \delta\mathbf{x}^i\phi^i$ which means that the value of the vector $\delta\mathbf{x}$ is interpolated form its value at the interpolation nodes, as the rest of the variables, using the same shape functions ϕ^i. Thus $\delta\mathbf{x}^i$ is only evaluated at the nodes i.

The first method proved a better behaviour.

8.1. Linear deformation field

There is a great freedom in the choice and invention of parametrizations. The most usual ones are based on a definition of the complete geometry by splines of all kinds and orders, (in aeronautical shape optimization, usually cubic B-splines, NURBS [27] or Bezier-curves [28]). In identification problems, the geometry is usually defined by simple geometrical entities, in turn defined by a few parameters (like ellipses defined by the coordinates of the center, the axes length and an angle of orientation in [29,30,6]).

A linear variation field is described by a constant deformation tensor (two parameters) plus a displacement of the field (four parameters making a total of 6). A definition of more physical meaning, in the sense that it comes from a deformation tensor, is the following:

$$\Theta^6_{ih} = \begin{bmatrix} 1 & 0 & x_2 & x_1 & x_1 & x_2 \\ 0 & 1 & -x_1 & x_2 & -x_2 & x_1 \end{bmatrix},$$

where $\mathbf{x} = \mathbf{x}^{\text{real}} - \mathbf{x}^{ch}$ ($\mathbf{x}$ with respect of the centroid of the flaw), i is the index for the direction and h is the index for the parameter, which gives each one a clear sense,

$$P_h = \begin{bmatrix} \delta x_1^{cg} \\ \delta x_2^{cg} \\ \delta\omega \\ \delta\varepsilon_m \\ \delta\varepsilon' \\ \delta\varepsilon_{12} \end{bmatrix} = \begin{bmatrix} \text{First coordinate of the centroid of the flaw} \\ \text{Second coordinate of the centroid of the flaw} \\ \text{Angle of rotation} \\ \text{Spherical strain} \\ \text{Horizontal elongation} \\ \text{Distortion} \end{bmatrix}.$$

8.2. Fourier parametrization

Ideally, a crack should be able to be represented by a curved line with a higher order than just quadratic, in order to adopt for example the shape of an S.

Besides, a lower number of parameters should be used as only deformations in the sense of the normal should be needed, eliminating all the tangential components that would appear, in a field defined with more generality in the x and y direction.

A parametrization based on a Fourier series decomposition has the following advantages:

- The ends of the crack are straight in the limit (zero curvature), maintaining the $\sqrt{r}$ behaviour of the crack tips.
- A Fourier series is capable of representing any shape with a sufficient number of terms.
- It is straightforward to add terms as the identification proceeds without need for redefining previous parameters, as would happen with Lagrange polynomials.
- Fourier series have good properties from the point of view of the regularization (see [31]).

The suggested parametrization is the following:

$$\Theta_{ih}^{\text{crack}} = \begin{bmatrix} 1-\xi & 0 & \xi & 0 & -\sin\alpha\sin 1\pi\xi & -\sin\alpha\sin 2\pi\xi & \cdots & -\sin\alpha\sin n\pi\xi \\ 0 & 1-\xi & 0 & \xi & \cos\alpha\sin 1\pi\xi & \cos\alpha\sin 2\pi\xi & \cdots & \cos\alpha\sin n\pi\xi \end{bmatrix},$$

where ξ is a normalized distance between the tips A and B, $\xi = \frac{(x_1-x_1^A)(x_1^B-x_1^A)+(x_2-x_2^A)(x_2^B-x_2^A)}{(x_1^B-x_1^A)^2+(x_2^B-x_2^A)^2}$ and $n = 1,\ldots,\infty$. $-\sin\alpha$ and $\cos\alpha$ are the director cosines of the segment that joins the crack tips (see Fig. 5).

8.3. Numerical evaluation

If the desired parametrization is substituted, $\delta x_i = \Theta_{ih}\delta P_h$, where Θ_{ih} is the parameterization matrix, and δP_h the vector of discrete parameter variations, the following expressions are derived:

$$\begin{aligned} \delta r_i &= (\Theta_{ih}(\xi) - \Theta_{ih}(x))\delta P_h, \\ \delta n_i &= t_i t_m t_l \epsilon_{mk}\Theta_{kg,l}\delta P_h, \\ \delta J &= t_k t_l \Theta_{lh,k}\delta P_h. \end{aligned} \tag{42}$$

Substituting (42) in (40), the systems of equations can be written as, δqBIE,

$$\begin{aligned} c_k^i\delta q_k(\boldsymbol{\xi}) + \int_\Gamma \Big[& d_{jk}^i(\mathbf{x},\boldsymbol{\xi})n_j(\boldsymbol{\xi})\delta q_k(\mathbf{x}) \\ & - s_{jkl}^i(\mathbf{x},\boldsymbol{\xi})n_j(\boldsymbol{\xi})n_l(\mathbf{x})\delta u_k(\mathbf{x})\Big]\mathrm{d}\Gamma(\mathbf{x}) \\ = {} & {}^g Q_h^i(\xi)\delta P_h, \end{aligned}$$

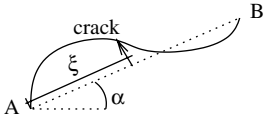

Fig. 5. Definition of the crack parametrization.

$$\begin{aligned} {}^g Q_h^i(\xi)\delta P_h = -\int_\Gamma \Big[& (d_{jk}^i(\mathbf{x},\boldsymbol{\xi})n_j(\boldsymbol{\xi})q_k(\mathbf{x}) \\ & - s_{jkl}^i(\mathbf{x},\boldsymbol{\xi})n_j(\boldsymbol{\xi})n_l(\mathbf{x})u_k)\delta J(\mathbf{x}) \\ & + (d_{jk}^i(\mathbf{x},\boldsymbol{\xi})q_k - s_{jkl}^i(\mathbf{x},\boldsymbol{\xi})n_l(\mathbf{x})u_k(\mathbf{x}))\delta n_j(\boldsymbol{\xi}) \\ & + (d_{jk,m}^i(\mathbf{x},\boldsymbol{\xi})n_j(\boldsymbol{\xi})q_k(\mathbf{x}) \\ & - s_{jkl,m}^i(\mathbf{x},\boldsymbol{\xi})n_l(\mathbf{x})n_j(\boldsymbol{\xi})u_k)\delta r_m(\mathbf{x},\boldsymbol{\xi}) \\ & - s_{jkl}^i(\mathbf{x},\boldsymbol{\xi})n_j(\boldsymbol{\xi})u_k\delta n_l(\mathbf{x})\Big]\mathrm{d}\Gamma(\mathbf{x}) \end{aligned}$$

which can also be written as

$$\mathbf{H}\delta\mathbf{u} - \mathbf{G}\delta\mathbf{q} = \boldsymbol{\Delta}\delta\mathbf{P}, \quad \Delta = {}^g Q_h^i(\xi),$$

where $\mathbf{u}$ and $\mathbf{q}$ are the displacement and stress vectors and $\mathbf{P}$ is the parameter set. $\mathbf{H}$ and $\mathbf{G}$ are identical to the system matrices in the usual BEM. $\boldsymbol{\Delta}$ is a matrix that groups the rest of the integrals, in which $\delta\mathbf{n}$, δJ and $\delta\mathbf{r}$ have to be substituted, and then $\delta\mathbf{P}$ becomes a common factor to be extracted. The evaluation of the kernels at singular points requires the use of special decompositions of the integrals, as detailed in Appendix B.

The application of the boundary conditions yield the same coefficients of the system matrix $\mathbf{A}$ as the usual BEM, since the prescribed values have zero variation. These variations are therefore not unknowns, as if they were prescribed

$$\mathbf{A}\delta\mathbf{v} = \boldsymbol{\Delta}\delta\mathbf{P},$$

where $\delta\mathbf{v}$ groups the non prescribed terms of $\delta\mathbf{u}$ and $\delta\mathbf{q}$ in the sequel, as done in the BEM. The solutions of the latter system for each column of $\boldsymbol{\Delta}$ can be performed and grouped into $\mathbf{J}$, which is called jacobian,

$$\delta\mathbf{v} = \mathbf{j}\delta\mathbf{P} \;\Rightarrow\; \mathbf{j} = \{j_{ih}\} = \frac{\mathrm{d}v_i}{\mathrm{d}P_h}.$$

This procedure is computationally low power-consuming since the system matrix $\mathbf{A}$ is already computed and factorized from the direct problem, and the remaining operations are the successive back and forward substitutions of the columns of $\boldsymbol{\Delta}$.

9. Solution of the inverse problem

The used solution strategy for the IP, stated as the computation of the parameters that best adjusts the response prediction from a numerical model to the real measurements, and formulated as a minimization problem of a cost functional $\mathscr{J}$ for the parameters P_h that characterize the defect. For that purpose, a residual vector $\mathbf{R} = \{R_i\}$ is defined to represent the discrepancy in the adjustment.

9.1. Residual

We introduce the *residual vector* $\mathbf{R}$ in order to quantify the discrepancy between the measurements and theoretical predictions. While the prediction is based on a set of h parameters P_h, the ideal measurement data can be denoted by a corresponding best adjusted set P_h^{r} where the superscript r denotes real defects,

$$R_i(P_h) = v_i(P_h) - v_i^{\mathrm{ex}}, \tag{44}$$

where v_i are the ith response to be measured (either displacements or tractions depending on the boundary conditions), first for the computed case $v_i(P_h)$, and second for the experimental measurements v_i^{ex}.

9.2. Cost functional

A cost functional $\mathscr{J}$ is defined in terms of the former residual R in a quadratic sense, which is also a least squares sense. This definition is meaningful from the statistical point of view, as well as from theory of linear algebra, since is minimizes distances in an Euclidean sense. The cost functional is hence defined as in Eq. (45) for the case of the discrete frequency domain

$$\mathscr{J} = \frac{1}{2}\mathbf{R}^{\mathrm{T}}\overline{\mathbf{R}} = \frac{1}{2}\|\mathbf{R}\|^2, \tag{45}$$

where T stands for the transpose in vectorial notation and $\overline{R}$ means the conjugate of the complex magnitude R.

9.3. Selection of minimization algorithm

A good survey on search or minimization algorithms can be found in Dennis and Schnabel [32] and others [33,34]. Among them, the most promising methods were tested in conjunction with the sensitivity supply and BEM for static measurements by Rus and Gallego [35,36]. It was shown that the Levenberg–Marquardt method usually coupled a higher convergence speed in terms of iterations with higher probability of success. The latter method has therefore been adopted as the standard in the sequel.

9.3.1. Levenberg–Marquardt and trust region approach (TRA)

By a multivariable Taylor series expansion of any function $f(\mathbf{x})$ until the second term, an affine model of $f(\mathbf{x}) : \Re^n \to \Re$ can be defined as

$$m_c(\mathbf{x}_c + \mathbf{p}) = f(\mathbf{x}_c) + \nabla f(\mathbf{x}_c)^{\mathrm{T}}\mathbf{p} + \frac{1}{2}\mathbf{p}^{\mathrm{T}}\nabla^2 f(\mathbf{x}_c)\mathbf{p} + h^{\mathrm{T}}h\epsilon(\mathbf{p}),$$

where $\nabla_i f = \frac{\partial f}{\partial x_i}$ is the gradient, $\nabla^2_{ij} f = \frac{\partial^2 f}{\partial x_i \partial x_j}$ is the Hessian, which will be symmetric if twice continuous differentiable.

The Levenberg–Marquardt method consists in an iterative algorithm in which from a starting guess $\mathbf{x}_k$ the following sequence is repeated:

(1) $(J_k^{\mathrm{T}}J_k - \mu_k I)\mathbf{s}_k = -J_k^{\mathrm{T}}R_k$ subject to $\|\mathbf{x}_{k+1} - \mathbf{x}_k\|_2 \leqslant \delta_k$,
(2) $\mathbf{x}_{k+1} = \mathbf{x}_k + \mathbf{s}_k$.

This is performed as described above in the model-trust region. This improves the behaviour of the algorithm for J with not full column rank. A line search can be added on this method, $\mathbf{x}_{k+1} = \mathbf{x}_k + \lambda_k \mathbf{s}_k$.

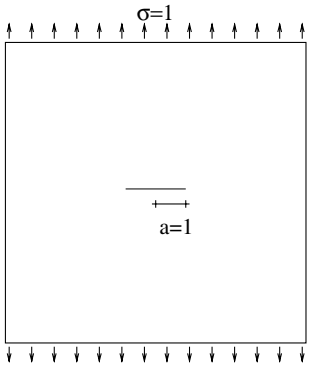

Fig. 6. Infinite plate with crack.

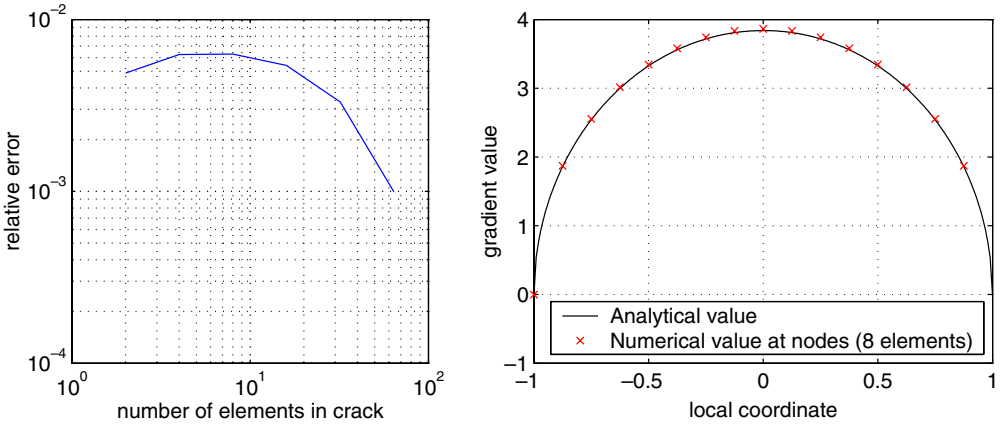

Fig. 7. Numerical and analytical comparison.

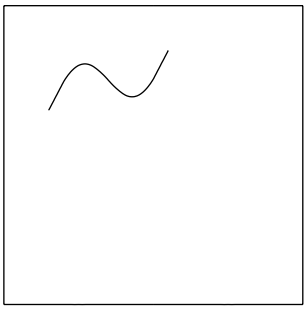

Fig. 8. Real scale description of crack benchmark.

The model-trust region consists in modifying H_k such that $\mathbf{s}_k \leqslant \delta_c$, i.e. s_k is within the trust radius δ_c. Primarily, the step may be chosen by the "hook" step (by $(H_c + \mu I)\mathbf{s}(\mu) = -\nabla f(\mathbf{x}_c)$), or, as in our case, by the double dogleg step, which is the point located at a distance δ_c of the line joining the Newton solution $(-H^{-1}\nabla f)$ with the Cauchy solution $\left(\frac{-\nabla f}{\|f\|}\right)$. Secondly, the trust region can be reduced by yet another backtracking of $f(\mathbf{x}_+) \leqslant f(\mathbf{x}_c) + \alpha\nabla f(\mathbf{x}_+ - \mathbf{x}_c)$.

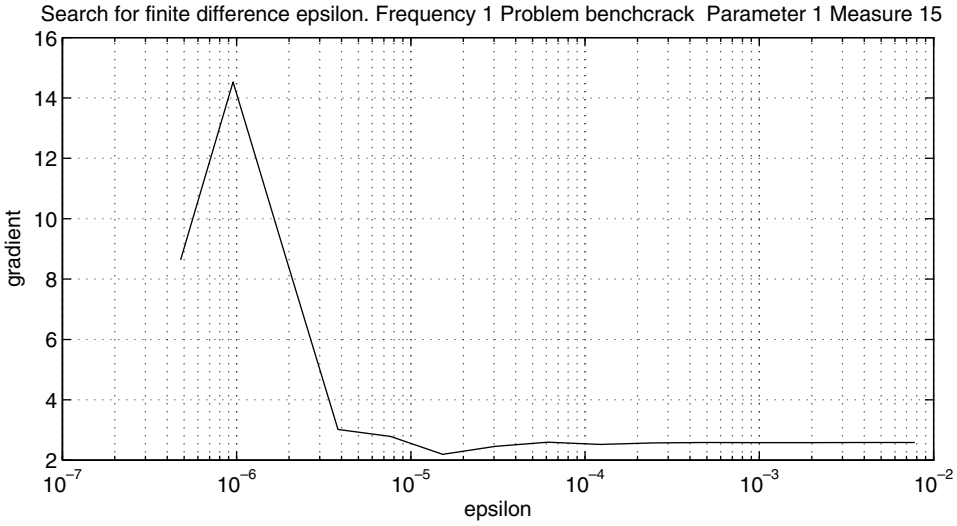

Fig. 9. Frequency. Test of finite difference distance. Value versus finite epsilon.

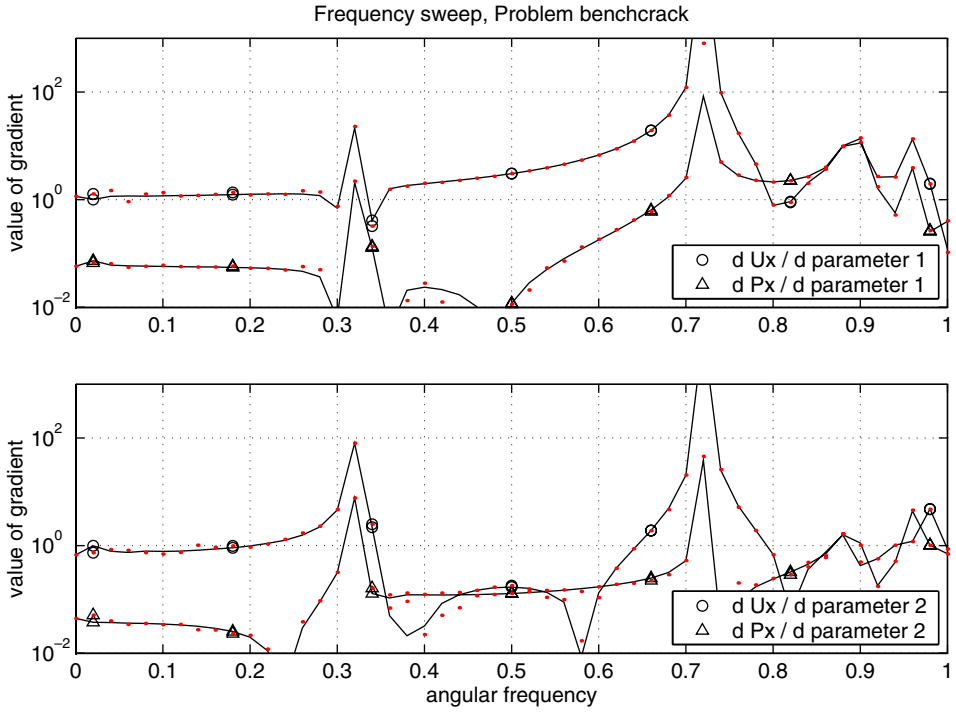

Fig. 10. Values of gradient. Crack problem. Continuous line: analytical value by direct derivation. Red dots: finite differences value. Each curve is the derivative with respect to the horizontal (1) and vertical (2) parameters. (For interpretation of the references in colour in this figure legend, the reader is referred to the web version of this article.)

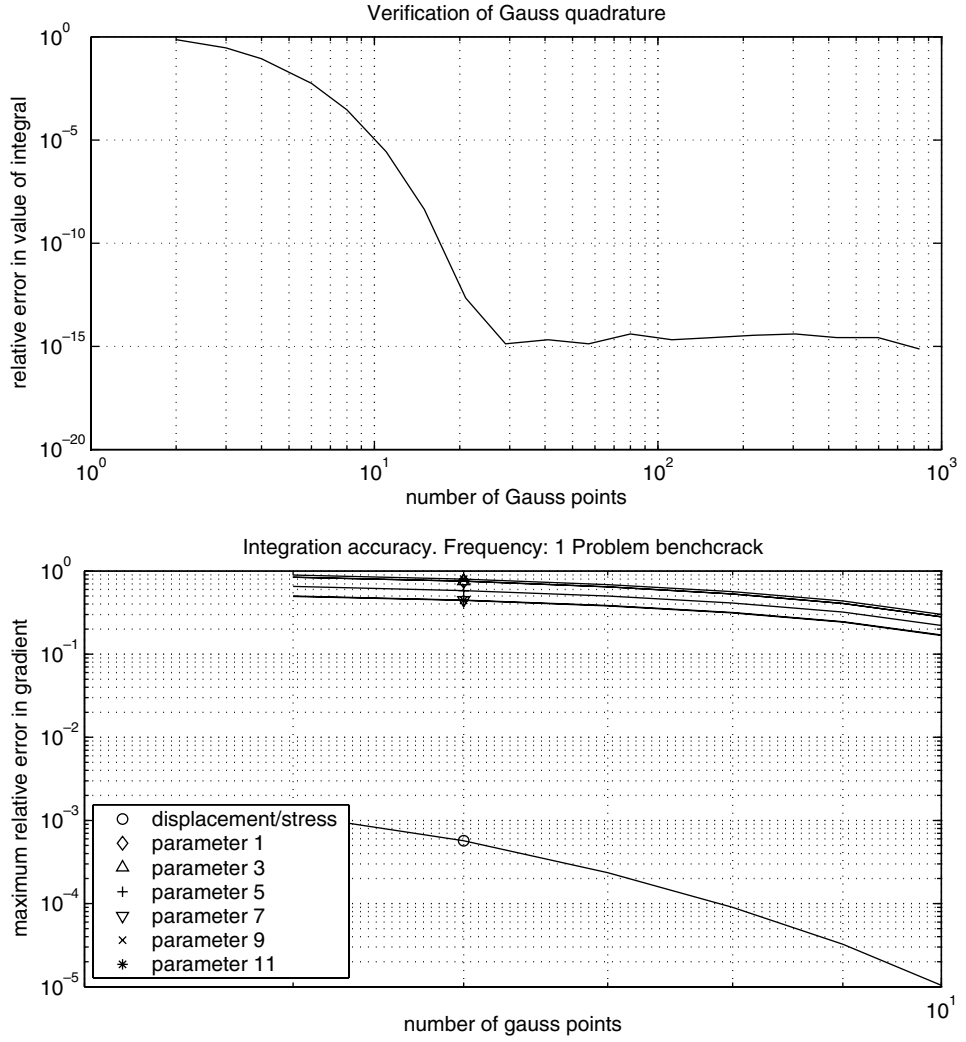

Fig. 11. Integration precision. Above: relative error in a hypersingular integral. Below: Error in the complete problem gradient calculation in the crack problem.

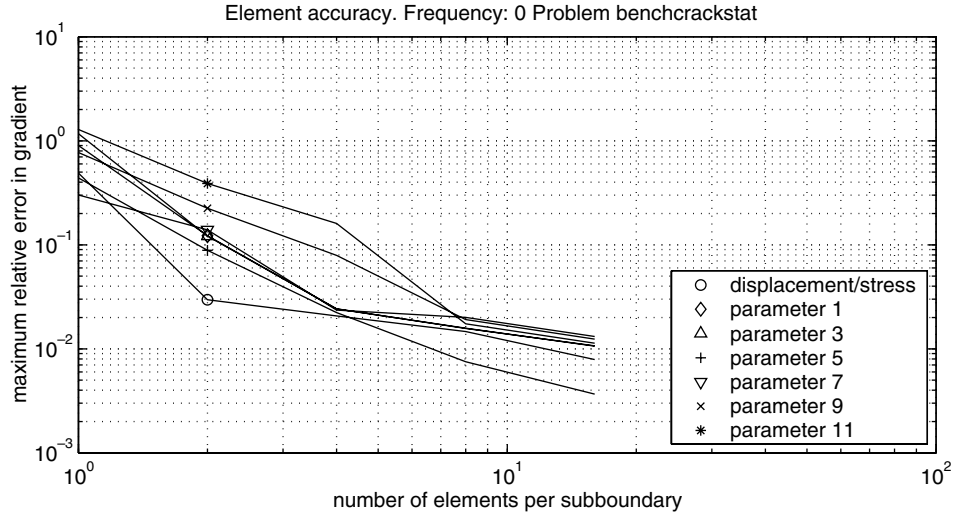

Fig. 12. Number of elements. Evolution of the relative error as the mesh is refined. Static problem.

9.3.2. Normalization

The normalization means a scaling of the problem in the sense that the units and magnitudes of the different parameters involved in the problem (for example the size of the flaw with respect to the total size, or the combination of displacement and stress measurements) may affect the solution.

Whereas Newton and BFGS methods are unaffected by scaling, the steepest descent and therefore the trust region models are affected. Therefore, the values introduced in the algorithms should previously be modified by an scaling matrix D_x in the form, $\hat{\mathbf{x}} = D_x\mathbf{x}$.

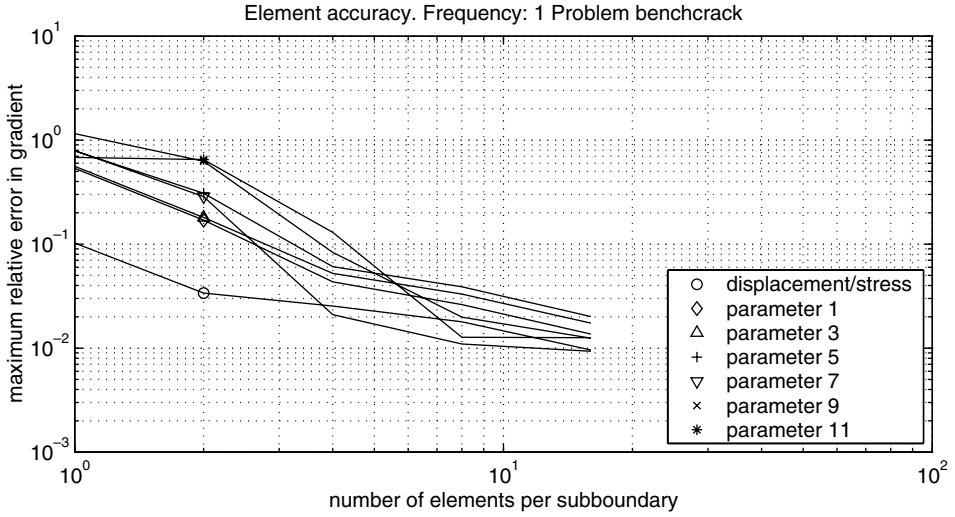

Fig. 13. Number of elements. Evolution of the relative error as the mesh is refined. Dynamic problem.

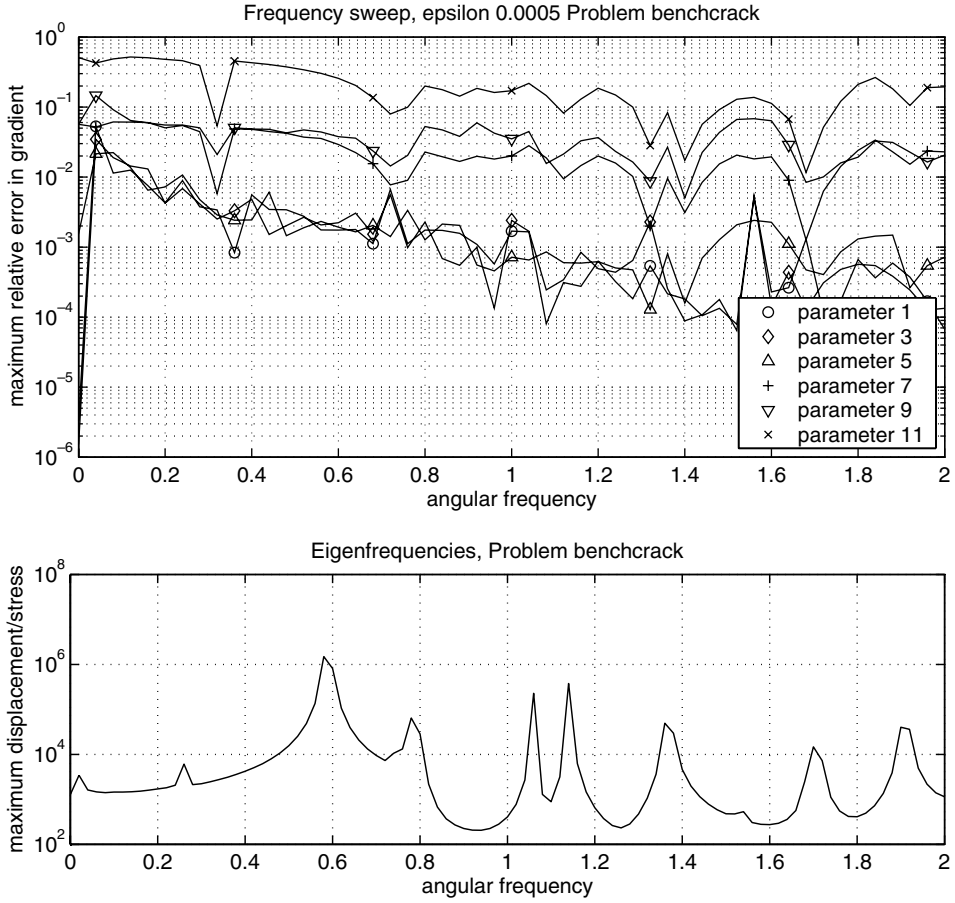

Fig. 14. Frequency. Relative error and eigenfrequencies.

There is a further effect that one should care. Too different magnitudes may also affect the conditioning of the matrices due to the computer precision, not only in the optimization algorithms, but also in the BEM calculations. The solution is similar as before.

9.3.3. Stopping

The stopping criteria is a relevant part of the iterative search algorithm. The properties of different stopping criteria in numerical optimization algorithms are the following. Both of the methods are used simultaneously.

- Step: $\frac{|\mathbf{x}_k-\mathbf{x}_{k-1}|}{\max\{\mathbf{x}_k,\text{typical}\mathbf{x}\}} \leqslant$ tolerance. The drawback of this method is that it may get stuck in local minima (or flat regions).
- Residual: $f \leqslant$ tolerance. The drawback of this method is that it requires the residual to become close to zero.

10. Sensitivity tests

10.1. Comparison with analytical solution. Direct derivation

The partial results corresponding to the sensitivity coefficients are verified here. A problem with a calculable analytical solution and sensitivity is the one consisting in a straight crack in an infinite medium subjected to an uniform stress from the end as shown in Fig. 6 can be found in many fracture mechanics books.

The displacements of the points on the lip of the crack follow:

$$u_x = 0,$$

$$u_y = \frac{a\sigma 2(1-\nu^2)}{E}\sqrt{1-\xi^2}$$

being ξ the local coordinate on the crack, which varies from -1 to 1.

The sensitivity to the semilength of the crack a in terms of the material derivative is, evaluated at the boundary of the hole

$$u_{x,a} = 0,$$

$$u_{y,a} = \frac{\sigma 2(1-\nu^2)}{E}\sqrt{1-\xi^2}.$$

The errors on the numerical calculations of these values at the middle point of the crack are shown in Fig. 7, for discretizations of the crack of 2, 4, 8, 16 and 32 elements. The value along the crack is also shown for a discretization of four elements.

Despite the simplicity of the model, the errors in the numerical figures remain low and converge properly as the mesh is refined.

10.2. Comparison with numerical solution. Direct derivation

The sensitivity tests are performed using a set of simple benchmark problems for the sake of reproductibility and simplility of comparison. The fixed contour consists of a 2×2 box of a material with constants $E = 1.0$; $\nu = 0.2$, $\rho = 1.0$. As boundary conditions the baseline is fixed and the upper side is subjected to an uniform unitary vertical stress. The crack starts from a straight and centered horizontal line of length 0.8, perturbed by the tip displacement and fourier parametrization vector $[-0.30, 0.30, -0.30, 0.70, 0.00, 0.20, 0.00, 0.00, 0.00, 0.00, 0.00, 0.00]$.

In the sequel, and unless other specifications are given, eight quadratic elements are used for the outer boundary and eight for the crack. The collocation points are always placed at $0.2a$ from the edge of the element, being a the distance between two geometrical, displacement or stress nodes.

10.2.1. Dependence of gradient value with frequency

The values of the gradients are shown at several structured points, in order to allow for the comparison. Two values are given for each benchmark problem,

(1) $\frac{\mathrm{d}u_x}{\mathrm{d}\Theta_n}$ is the variation of the horizontal displacement of the middle point on the upper side when parameter n grows (see Section 8.1).
(2) $\frac{\mathrm{d}p_x}{\mathrm{d}\Theta_n}$ is the variation of the horizontal stress vector of the middle point on the lower side when parameter n grows.

These values were computed using 32 elements for the outer boundary and 32 for the crack. The distance for the finite differences is set to $\frac{0.002}{\omega}$. The division by ω is justified by the equivalent scaling that the change of frequency implies in the fundamental solutions. The presence of eigenfrequencies, gives a jagged aspect to the graphics. An estimation of the same value using finite differences is made, superimposing it by dots. A perfect agreement is shown visually, proving that the right value is being calculated. Therefore, the converging solution for refined meshes should give the converged solution.

10.2.2. Integration precision

In order to have control over the sources of error we now study the accuracy of the integration of the boundary

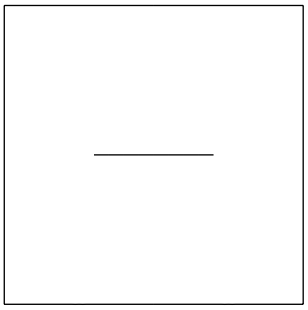

Fig. 15. Description of crack benchmark. Initial guess.

integral equations. To do this, the Gauss quadrature is modified.

From Fig. 11 the convergence of an hypersingular integral (first) and two benchmark problems by increasing the number of integration points is confirmed. The reference value is an integral with an extremely high number of points (2500 gauss points for the first and 10 gauss points combined with an 8× refinement of the discretization).

10.2.3. Number of elements

To finish the study of integration accuracy, the discretization is varied by increasing the number of elements. Figs.

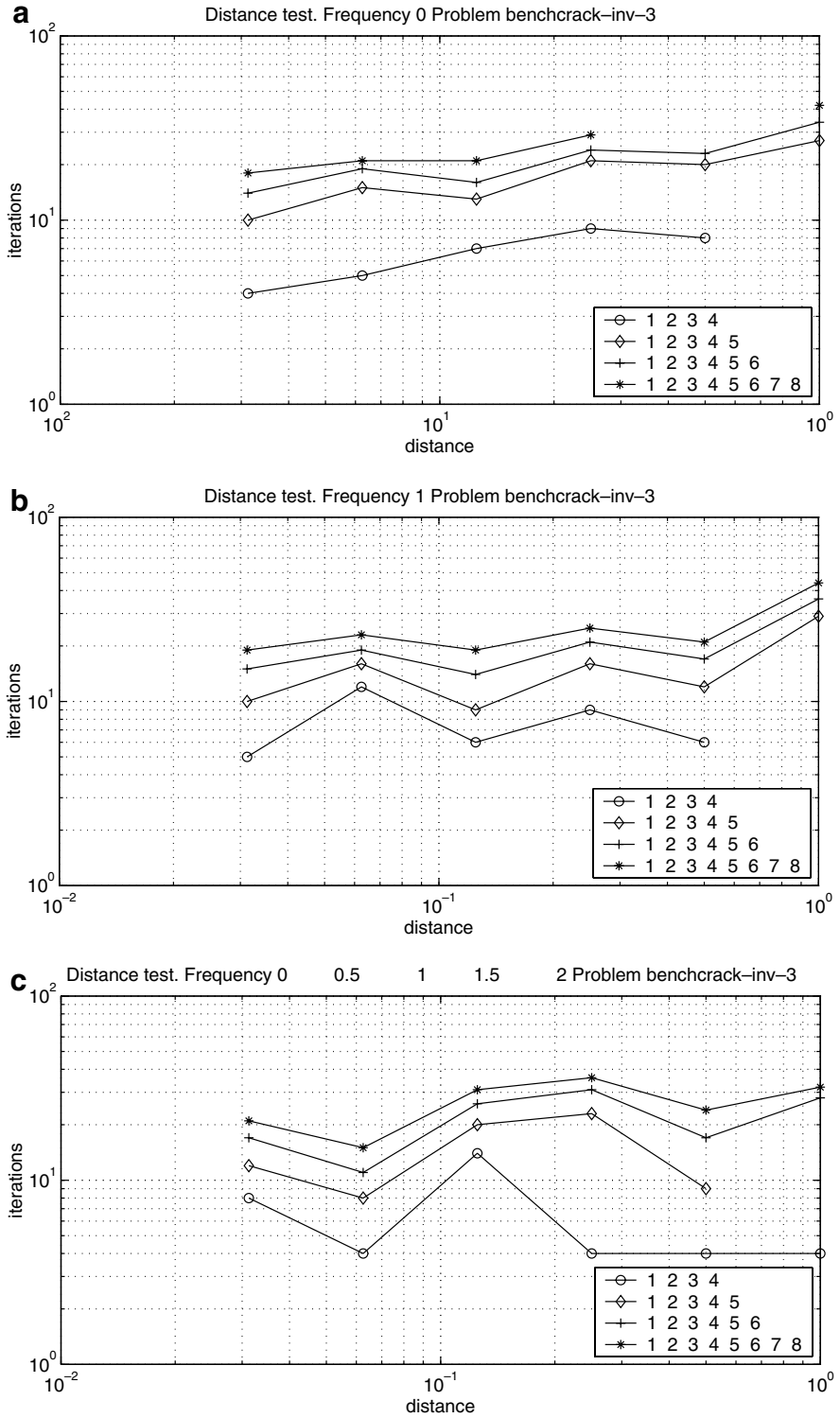

Fig. 16. Convergence with distance from actual flaw: (a) static excitation, (b) single frequency excitation ($\omega = 1.0$), (c) multiple frequency excitation ($\omega = 0.0, 0.5, 1.0, 1.5, 2.0$).

12 and 13 prove a clear convergence of the solution by increasing the refinement of the mesh. The reference value is taken from a sufficiently refined mesh.

10.2.4. Influence of frequency

From Fig. 9 the epsilon (finite difference distance) chosen for all the frequency comparisons is 10^{-4}. The errors measured in Fig. 14 are the comparison between the analytic gradient and the one obtained by centered finite differences. The eigenfrequencies are also shown to visualize the relationship between the errors at the edge of the eigenfrequencies, which may cause the finite difference calculations to diverge. It is shown that the errors are low even for frequencies comparable to the first eigenfrequency (see Fig. 10).

Unlike other examples, the reference value need not be close to the exact solution of the physical problem, but to the finite difference estimation for the same level of meshing. Crack problems show higher discordancies. Looking closer at the figure, this only appears to happen for the last parameters, which involve highly warped geometries. As seen in the following figures, there are higher errors at a low number of elements, but all are rapidly reduced by a sufficient mesh refinement. Another relevant effect is that the errors become higher at low frequencies, which may be due to the numerical difficulties for the numerical convergence of the dynamic fundamental solutions of the BEM to the static ones in the 2D case.

11. Inverse problem solution

11.1. Convergence tests using Levenberg–Marquardt algorithm and direct derivation

The benchmark problem used at the sensitivity test by direct differentiation is used for the complete solution of an identification inverse problem using a least squares minimization algorithm: the Levenberg–Marquardt method with line search and gradient supply.

The starting configuration or initial guess is the corresponding to Fig. 15. The final configuration to be sought is shown in Fig. 8.

The fixed boundary consists of a 2×2 box of a material with constants $E = 1.0$; $v = 0.2$, $\rho = 1.0$. As boundary conditions the baseline is fixed and the upper side is subjected to an uniform unitary vertical stress. The initial crack is a horizontal centered segment of length 0.8, and the final crack is defined by $x = -0.7 + 0.8\lambda$; $y = 0.3 + 0.4\lambda + 0.2\sin(2\pi\lambda)$, where the parameter λ goes from 0 to 1. The discretization is the same as for the sensitivity tests. The used parametrization is the fourier crack parametrization.

The identification is made increasing gradually the number of parameters. They are increased stepwise in so called restarts. In each of them, the search algorithm is run for a particular subset of the parameters, and leaving the remaining fixed at zero value. In the following step, the search algorithm is run again with an increased subset of parameters, and using as initial guess the output value in the preceding step. A total of four restarts are carried out, selecting the parameters listed in the legend. The maximum number of iterations per restart is limited to 20, and the maximum increment in the value of each parameter is limited to 0.2 in order to limit possible divergences, using the *arcTan* remapping. The stopping criteria is $\Delta P = 0.001$.

Three plots are made for each benchmark problem: one corresponding to the search with static data; one corresponding to the values at frequency $\omega = 1.0$, and a third graphic with simultaneous data measured at frequencies $\omega = \{0.0, 0.5, 1.0, 1.5, 2.0\}$.

11.1.1. Relationship between convergence and distance

The scope of convergence for each problem at each frequency is verified in this section. For this purpose, the

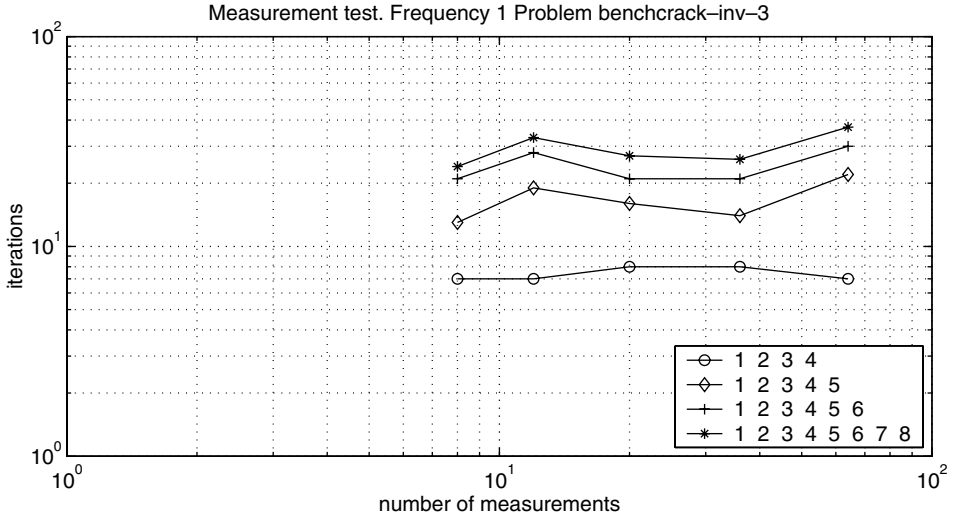

Fig. 17. Convergence with different number of measurements and parameters.

number of iterations (when converged) are plot for a number of initial guess distances from the real solution. This distance is simply defined by scaling the parameter vector that defines the initial configuration from the final one. Fig. 16 shows the necessary iterations for the convergence placing the initial guess at a proportional value between

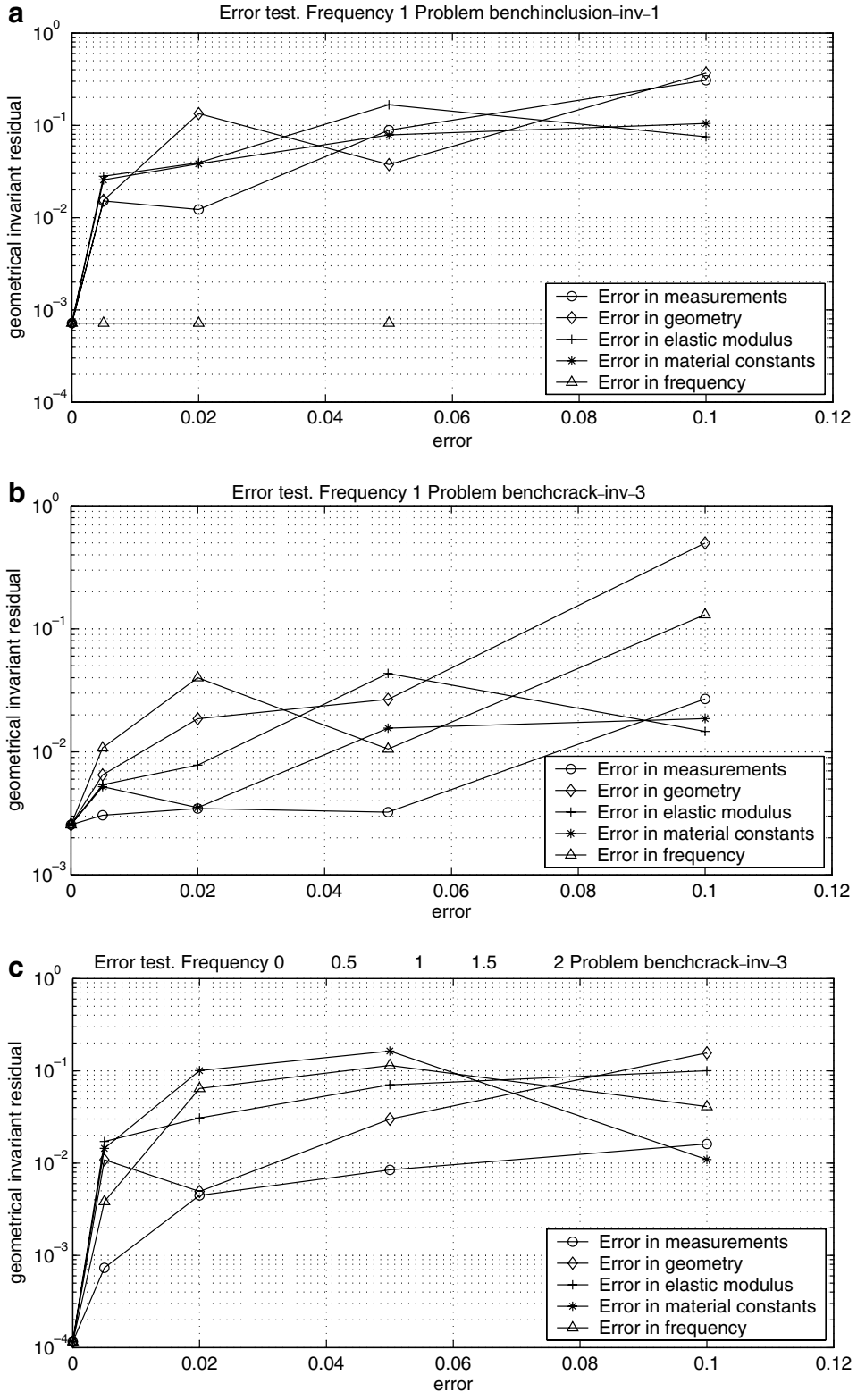

Fig. 18. Convergence with errors: (a) static excitation, (b) single frequency excitation ($\omega = 1.0$), (c) multiple frequency excitation ($\omega = 0.0, 0.5, 1.0, 1.5, 2.0$).

the zero-vector and the final parameter. In the case of absence of convergence, the corresponding point is not plotted. It should be noted that the convergence is not necessary to the real result. The partial results at each restart are plotted.

One may observe that the necessary iterations increase more or less gradually with the distance and consequent difficulty of the search. A high number of iterations is needed for the search of cracks, even at simple parametrizations.

Another interesting point is that, as expected, the success in a particular restart is critical for the success of the following one. This justifies the used dosage of parameters.

11.1.2. Dependence on the measurements

The number of data supply for an inverse problem is an important factor. Here we solve the problems with a varying number of measurements: from a minimum of 8 (on the half right vertical side), and increasing anti-clockwise along the outer boundary until 64.

Fig. 17 is made for frequency $\omega = 1.0$. The starting guess is placed at an equivalent distance of 0.2. The number of measurements does not seem to imply important effects in the process of convergence. It should be noted that, unless special regularization techniques are used, the number of measurement data should be equal or higher than the number of parameters in order to allow for the convergence to a realistic solution.

11.1.3. Dependence on the errors

In order to simulate real cases, some errors are introduced in all parts of the model: measurements, geometry (alteration of the coordinates of each node), elastic modulus, other elastic constants, and frequency. The errors are defined by a normal distribution of zero mean and variance defined by the error.

Fig. 18 shows in the vertical axis the final value (i.e. after search convergence) of the sum of geometrical invariants error (length, center of gravity, and the 2D intertias, which gives an indication of how different the guess is from the real defect) when the problem has a particular value in the error on either the measurements, the geometry, the elastic modulus, the other material constants or the frequency, for each curve respectively. The unitary value of the error is tested at values of 0, 0.005, 0.02, 0.05, 0.10 (i.e., up to 10%).

These examples show that the fitness of the final estimation is rapidly distorted even at small errors, but looking at the values of the error, the estimation is reasonable, considering the ill-posedness of the IIP problem.

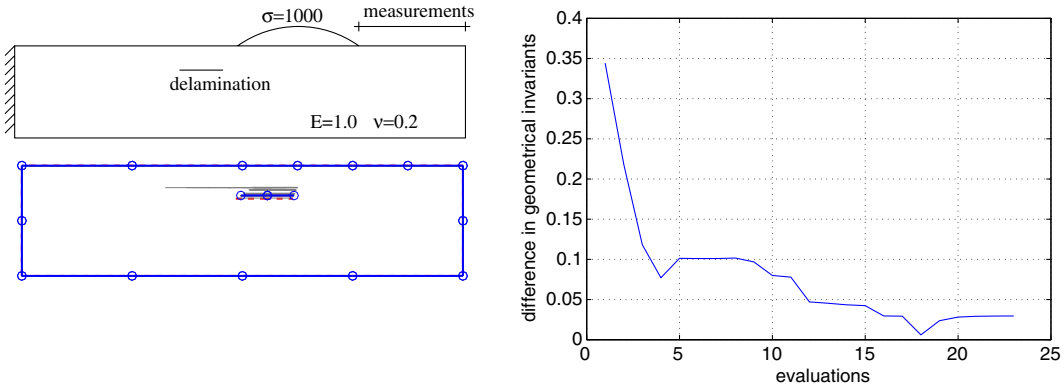

Fig. 19. Crack identification in a beam: five measurements. Left: definition of the model and iterations. Right: Geometrical error.

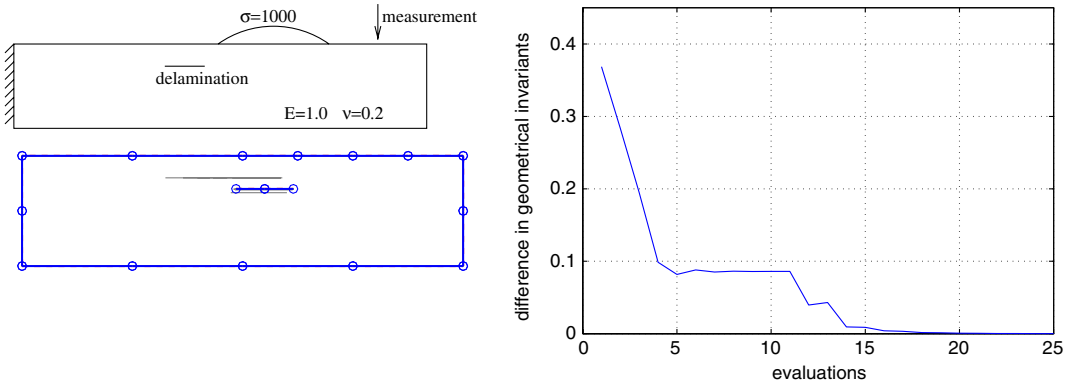

Fig. 20. Crack identification in a beam: one measurement. Left: definition of the model and iterations. Right: Geometrical error.

12. Identification of delamination crack position and length in a beam

This sample problem simulates the search and control of a crack that appears on a bending beam of size 5×1 with the mechanical properties shown in Fig. 19. In addition, the density is 1.0 and the damping ratio 10% throughout, for frequency $\omega = 1.0$. A set of five nodes is measured, on the area shown in figure of the first case, when a parabolic load is applied beside, whereas the second case is solved for a single measurement of the vertical displacement at the depicted node.

This may simulate the search of a delamination in an isotropic composite beam of an airplane wing, for instance. In Fig. 19 the correct convergence is shown after $7 + 7$ iterations in a first step that allows horizontal movement, and a second step with all three parameters.

The wave analysis is used as before to this example, giving the results in Fig. 20. A good convergence is obtained after $11 + 15$ iterations.

13. Conclusions

A procedure for obtaining the gradient or sensitivity of hypersingular boundary integral equations, the *qBIE* used in the BEM (which is also valid for the *uBIE*) is developed. The sensitivity is obtained analytically before discretization, and before parametrization, with respect to a generic differential variation field of the geometry.

The conditions required by all the kernels, weights, discretization and parametrization are studied, assuring the applicability. Besides, all the necessary tools for the numerical implementation have been developed and tested.

The numerical values converge well in statics and steady state dynamics, both in simple and complex problems. The convergence of the gradient values while improving the discretization is steady in every example, at similar rates to the solution of the direct problems. This fact together with a visually identical value in comparison with the gradient estimation by finite differences indicates that the correct values are being obtained.

In fact, the finite differences (FD) method seems to fail in the low frequency dynamic problems, since a large finite distance amplifies second order effects, whereas small values are unstabilizing rapidly due to low frequency-related numerical inaccuracies in the direct problem. This inaccuracy together with the higher computational cost of FD recommends the use of direct differentiation.

The functionality is confirmed by the application to the solution of complete inverse problems by the Levenberg–Marquardt method. The test of convergence has been made including all the possible errors: measurement, model, geometry and frequency, attaining good results. The scope of convergence has been systematically studied by exploring the range of distances from which the correct solution is reached, in order to show the capabilities and reliability of the method.

Finally, a technique for identification based on the study of the steady state waveform is presented. It consists on the harmonic decomposition of the response to a non-sinusoidal harmonic excitation. This allows the measurement of only one point, and allows for much lower computational cost than transient analysis, as well as higher precision in the measurements.

Appendix A. Free terms

A.1. Order of singularity

The basic integral equations before the limit to the boundary (for $\boldsymbol{\xi}$ internal) are the following, and the order of each integrand when $\boldsymbol{\xi}$ approaches $\mathbf{x}$ are studied for a correct treatment of the integrals.

qBIE:

$$\delta^i_k q_k(\boldsymbol{\xi}) + \int_\Gamma \left[d^i_{jk}(\mathbf{x},\boldsymbol{\xi}) n_j(\boldsymbol{\xi}) q_k(\mathbf{x}) - s^i_{jkl}(\mathbf{x},\boldsymbol{\xi}) n_j(\boldsymbol{\xi}) n_l(\mathbf{x}) u_k(\mathbf{x}) \right] \mathrm{d}\Gamma(\mathbf{x}) = 0 \quad (\boldsymbol{\xi} \text{ internal})$$

Integrand	Order
$s^i_{jkl}(\mathbf{x},\boldsymbol{\xi}) n_j(\boldsymbol{\xi}) n_l(\mathbf{x}) u_k(\mathbf{x})$	r^{-2}
$d^i_{jk}(\mathbf{x},\boldsymbol{\xi}) n_j(\boldsymbol{\xi}) q_k(\mathbf{x})$	r^{-1}

$\delta qBIE$:

$$\begin{aligned}
&\delta^i_k \delta q_k(\boldsymbol{\xi}) + \int_\Gamma [d^i_{jk}(\mathbf{x},\boldsymbol{\xi}) n_j(\boldsymbol{\xi}) \delta q_k(\mathbf{x}) \\
&- s^i_{jkl}(\mathbf{x},\boldsymbol{\xi}) n_j(\boldsymbol{\xi}) n_l(\mathbf{x}) \delta u_k(\mathbf{x})] \, \mathrm{d}\Gamma(\mathbf{x}) \\
&+ \int_\Gamma [(d^i_{jk}(\mathbf{x},\boldsymbol{\xi}) n_j(\boldsymbol{\xi}) q_k(\mathbf{x}) - s^i_{jkl}(\mathbf{x},\boldsymbol{\xi}) n_j(\boldsymbol{\xi}) n_l(\mathbf{x}) u_k) \delta J(\mathbf{x}) \\
&+ (d^i_{jk}(\mathbf{x},\boldsymbol{\xi}) q_k - s^i_{jkl}(\mathbf{x},\boldsymbol{\xi}) n_l(\mathbf{x}) u_k(\mathbf{x})) \delta n_j(\boldsymbol{\xi}) \\
&+ (d^i_{jk,m}(\mathbf{x},\boldsymbol{\xi}) n_j(\boldsymbol{\xi}) q_k(\mathbf{x}) - s^i_{jkl,m}(\mathbf{x},\boldsymbol{\xi}) n_l(\mathbf{x}) n_j(\boldsymbol{\xi}) u_k) \delta r_m(\mathbf{x},\boldsymbol{\xi}) \\
&- s^i_{jkl}(\mathbf{x},\boldsymbol{\xi}) n_j(\boldsymbol{\xi}) u_k \delta n_l(\mathbf{x})] \, \mathrm{d}\Gamma(\mathbf{x}) \\
&= 0 \quad (\boldsymbol{\xi} \text{ internal})
\end{aligned}$$

Integrand	Order
$s^i_{jkl} n_j(\boldsymbol{\xi}) u_k \delta n_l(\mathbf{x})$	r^{-2}
$t^i_{jkl,m} n_l(\mathbf{x}) n_j(\boldsymbol{\xi}) u_k \delta r_m$	r^{-2}
$s^i_{jkl} n_j(\boldsymbol{\xi}) n_l(\mathbf{x}) \delta u_k$	r^{-2}
$-d^i_{jk,m} n_j(\boldsymbol{\xi}) q_k \delta r_m$	r^{-1}
$-d^i_{jk} n_j(\boldsymbol{\xi}) \delta q_k$	r^{-1}
$s^i_{jkl} n_j(\boldsymbol{\xi}) n_l(\mathbf{x}) u_k \delta J$	r^{-2}
$-d^i_{jk} n_j(\boldsymbol{\xi}) q_k \delta J$	r^{-1}
$s^i_{jkl} n_l(\mathbf{x}) u_k \delta n_j(\boldsymbol{\xi})$	r^{-2}
$-d^i_{jk} q_k \delta n_j(\boldsymbol{\xi})$	r^{-1}

A.2. Free terms calculation

The resulting free terms are the following, in the case of a smooth boundary at the collocation point.

A.2.1. Free terms for the qBIE

$$(1)\quad \lim_{\varepsilon\to 0^+}\int_{s_\varepsilon} s^i_{jkl}(\mathbf{x},\boldsymbol{\xi})n_j(\boldsymbol{\xi})n_l(\mathbf{x})u_k(\mathbf{x})\,\mathrm{d}\Gamma = n_l u_j IQ1^i_{jl}\lim_{\varepsilon\to 0^+}\frac{1}{\varepsilon} + n_l u_{j,k} Q1^i_{jkl},$$

$$(2)\quad \lim_{\varepsilon\to 0^+}\int_{s_\varepsilon} d^i_{jk}(\mathbf{x},\boldsymbol{\xi})n_j(\boldsymbol{\xi})q_k(\mathbf{x})\,\mathrm{d}\Gamma = n_l\sigma_{jk}Q2^i_{jkl}.$$

The terms $n_l u_{j,k}Q1^i_{jkl} + n_l\sigma_{jk}Q2^i_{jkl}$ group into $-\frac{1}{2}\delta^i_k q_k(\boldsymbol{\xi})$ taking into account that $q_k = \sigma_{jk}n_j(\mathbf{x}) = (\lambda\delta_{jk}u_{m,m} + \mu(u_{k,j}+u_{j,k}))n_j(\mathbf{x})$.

In the *qBIE* and δ*qBIE* there are some terms that tend to infinite when the radius ε disappears (terms in $\lim_{\varepsilon\to 0^+}\frac{1}{\varepsilon}$). Since all equations should take finite values in order to have a physical sense, the sum of all those terms cancel out with similar divergent terms in the integral along $\Gamma - \Gamma_\varepsilon$. The infinite terms are named with a starting initial *I* (e.g. *IQ*1 is the Infinite free term of the *qBIE* number 1).

A.2.2. Free terms for the δqBIE

$$(1)\quad \lim_{\varepsilon\to 0^+}\int_{s_\varepsilon} s^i_{jkl}n_j(\boldsymbol{\xi})u_k\delta n_l(\mathbf{x})\,\mathrm{d}\Gamma = n_j u_k\delta x_{l,m}IDQ1^i_{jklm}\lim_{\varepsilon\to 0^+}\frac{1}{\varepsilon} + n_j u_{k,m}\delta x_{l,n}DQ1^i_{jklmn} + n_j u_k\delta x_{l,mn}DQ5^i_{jklmn},$$

$$(2)\quad \lim_{\varepsilon\to 0^+}\int_{s_\varepsilon} s^i_{jkl,m}n_l(\mathbf{x})n_j(\boldsymbol{\xi})u_k\delta r_m\,\mathrm{d}\Gamma = n_j u_k\delta x_{l,m}IDQ2^i_{jklm}\lim_{\varepsilon\to 0^+}\frac{1}{\varepsilon} + n_j u_{k,m}\delta x_{l,n}DQ2^i_{jklmn} + n_j u_k\delta x_{l,mn}DQ6^i_{jklmn},$$

$$(3)\quad \lim_{\varepsilon\to 0^+}\int_{s_\varepsilon} s^i_{jkl}n_j(\boldsymbol{\xi})n_l(\mathbf{x})\delta u_k\,\mathrm{d}\Gamma = n_l u_j IQ1^i_{jl}\lim_{\varepsilon\to 0^+}\frac{1}{\varepsilon} + n_l\delta u_{j,k}DQ11^i_{jkl},$$

$$(4)\quad \lim_{\varepsilon\to 0^+}\int_{s_\varepsilon} -d^i_{jk,m}n_j(\boldsymbol{\xi})q_k\delta r_m\,\mathrm{d}\Gamma = n_j\sigma_{km}\delta x_{l,n}DQ8^i_{jklmn},$$

$$(5)\quad \lim_{\varepsilon\to 0^+}\int_{s_\varepsilon} -d^i_{jk}n_j(\boldsymbol{\xi})\delta q_k\,\mathrm{d}\Gamma = n_l\delta\sigma_{jk}DQ12^i_{jkl} + \delta n_l\sigma_{jk}DQ13^i_{jkl},$$

$$(6)\quad \lim_{\varepsilon\to 0^+}\int_{s_\varepsilon} s^i_{jkl}n_j(\boldsymbol{\xi})n_l(\mathbf{x})u_k\delta J\,\mathrm{d}\Gamma = n_j u_k\delta x_{l,m}IDQ3^i_{jklm}\lim_{\varepsilon\to 0^+}\frac{1}{\varepsilon} + n_j u_{k,m}\delta x_{l,n}DQ3^i_{jklmn} + n_j u_k\delta x_{l,n}DQ7^i_{jklmn},$$

$$(7)\quad \lim_{\varepsilon\to 0^+}\int_{s_\varepsilon} -d^i_{jk}n_j(\boldsymbol{\xi})q_k\delta J\,\mathrm{d}\Gamma = n_j\sigma_{km}\delta x_{l,n}DQ9^i_{jklmn},$$

$$(8)\quad \lim_{\varepsilon\to 0^+}\int_{s_\varepsilon} s^i_{jkl}n_l(\mathbf{x})u_k\delta n_j(\boldsymbol{\xi})\,\mathrm{d}\Gamma = \delta n_l u_j IDQ4^i_{jl}\lim_{\varepsilon\to 0^+}\frac{1}{\varepsilon} + \delta n_l u_{j,k}DQ4^i_{jkl},$$

$$(9)\quad \lim_{\varepsilon\to 0^+}\int_{s_\varepsilon} -d^i_{jk}q_k\delta n_j(\boldsymbol{\xi})\,\mathrm{d}\Gamma = \delta n_l\sigma_{jk}DQ10^i_{jkl}.$$

The terms $\delta n_l u_{j,k}DQ4^i_{jkl} + \delta n_l\sigma_{jk}DQ10^i_{jkl}$ group into $-\frac{1}{2}\delta^i_k\sigma_{kl}(\boldsymbol{\xi})\delta n_l(\boldsymbol{\xi})$ taking into account that $q_k = \sigma_{jk}n_j(\mathbf{x}) = (\lambda\delta_{jk}u_{m,m} + \mu(u_{k,j}+u_{j,k}))n_j(\mathbf{x})$.

Terms $n_l\delta u_{j,k}DQ11^i_{jkl} + n_l\delta\sigma_{jk}DQ12^i_{jkl}$ also group into $-\frac{1}{2}\delta^i_k\delta\sigma_{kl}(\boldsymbol{\xi})n_l(\boldsymbol{\xi})$ for the same reason. These last two grouped terms reduce further to $-\frac{1}{2}\delta^i_k\delta q_k$.

The sum of terms in $DQ8^i_{jklmn}, DQ9^i_{jklmn}, DQ13^i_{jkl}$ should be equal to zero, although this has still not been confirmed analytically.

It would make no sense to write the δ*qBIE* for non-smooth points since it should be written for points within the elements, which are smooth.

Appendix B. Regularization of integrals

When the collocation point is not placed on the integrated element, a regular Gauss quadrature formula can be utilized.

B.1. Singular points

As it uses to happen with integral equation methods, the integrals have singularities of different orders. After the limiting process the integrals are defined outside the *artificial ball* around the pole, and divided into a first one that may have a singularity, and turns to be a Cauchy Principal Value (CPV: $\int_a^b CPV = \lim_{\epsilon\to 0}(\int_a^{-\epsilon} + \int_\epsilon^b)$), and a second integral that tends to a so called free term, calculated in the appendix:

$$\int_\Gamma f\,\mathrm{d}\Gamma = \lim_{\epsilon\to 0}\left(\int_{\Gamma-\Gamma_\epsilon} f\,\mathrm{d}\Gamma\right) + \lim_{\epsilon\to 0}\left(\int_{\Gamma_\epsilon} f\,\mathrm{d}\Gamma\right).$$

When some values at this point tend to infinite, the first term has singularities: $\log\frac{1}{x}$, $\frac{1}{x}$, $\frac{1}{x^2}$. In order to be able to compute them numerically in an efficient way, we need to use a combination of two techniques:

- Decomposing the kernel in a sum of a regular part (continuous and differentiable, and not tending to infinite), which will be integrated numerically, and a simpler singular part, to be integrated analytically ($\int = \int_{\text{regular}} + \int_{\text{analytic}}$).
- Placing the collocation points a bit separated from the ends of the elements when necessary. As proved later, this will not be needed for this formulation as long as the varying geometry is smooth.
- Integrating by special gauss quadratures:

$$\int \ln\left(\frac{1}{x}\right) f(x)\,\mathrm{d}\Gamma(x) = \sum_{g=\text{gauss}} \omega_g^{\ln} f(\xi_g^{\ln})J.$$

The four different types of integrals that arise here are computed as follows:

B.2. Regular

This arises when the kernel of the integral is bounded and Holder continuous, with finite derivative in the whole range. We use a simple gauss quadrature with a variable change:

$$\int_\Gamma f(s)\,\mathrm{d}s = \int_{-1}^{1} J(\xi) f(s(\xi))\,\mathrm{d}\xi = \sum_{g=\text{gauss}} J(\xi)\omega_g f(s(\xi_g)).$$

B.3. Log-singular

This appears when the integral has the form $\int_\Gamma f(s) + g(s)\log\frac{1}{r(s)}\,\mathrm{d}s$, where f and g are also bounded and Holder continuous. We utilize the special gauss quadrature

$$\begin{aligned}\int_\Gamma f(s) + g(s)\log\frac{1}{r(s)}\,\mathrm{d}s &= \sum_{g=\text{gauss}} J(\xi)\omega_g f(s(\xi_g)) \\ &+ \sum_{g=\text{gauss}} J(\xi)\omega_g g(s(\xi_g))\log\left(\frac{\mathrm{Abs}(\xi_g - \mathrm{nod})J(\xi)}{rJ^{\ln}(\xi)}\right) \\ &+ \sum_{g=\text{gauss}}^{\text{left}} J^{\ln}\omega^{\ln}\frac{g(s(\xi_g^{\ln}))}{\log\frac{1}{r}} + \sum_{g=\text{gauss}}^{\text{right}} J^{\ln}\omega^{\ln}\frac{g(s(\xi_g^{\ln}))}{\log\frac{1}{r}},\end{aligned}$$

where $J^{\ln}(\xi) = J(\xi)(1 + \mathrm{Abs}(\mathrm{nod}))$, and nod is the value of ξ where the singularity appears.

B.4. $\frac{1}{r}$ Singular

This means that the integral has the form $\int_\Gamma \frac{f(s)}{r(s)}\,\mathrm{d}s$, where f is again bounded and Holder continuous. Two methods are mainly used in the literature, one from Gallego [37],

$$\begin{aligned}\int_a^b \frac{f(s)}{r(s)}\,\mathrm{d}s &= \int_a^b \frac{f(s) - f(s_0)\frac{\mathrm{d}r}{\mathrm{d}s}}{r(s)}\,\mathrm{d}s + f(s_0)\int_a^b \frac{\mathrm{d}r}{\mathrm{d}s}\frac{1}{r(s)}\,\mathrm{d}s \\ &= \int_a^b \frac{f(s) - f(s_0)\frac{r_i(s)\frac{\partial y_i(s)}{\partial\xi}}{r(s)J(s)}}{r(s)}\,\mathrm{d}s + f(s_0)(\mathrm{Ln}(r(b)) \\ &\quad - \mathrm{Ln}(r(a)))\end{aligned}$$

and one from Guiggiani [38]

$$\begin{aligned}\int_a^b \frac{f(s)}{r(s)}\,\mathrm{d}s &= \int_a^b \left(\frac{f(s)}{r(s)} - \frac{f(s_0)\frac{\mathrm{d}\xi}{\mathrm{d}s}}{\xi - \xi_0}\right)\mathrm{d}s \\ &\quad + f(s_0)\int_a^b \frac{\mathrm{d}\xi}{\mathrm{d}s}\frac{1}{\xi - \xi_0}\,\mathrm{d}s \\ &= \int_a^b \left(\frac{f(s)}{r(s)} - \frac{f(s_0)}{J(s)(\xi - \xi_0)}\right)\mathrm{d}s \\ &\quad + f(s_0)(\mathrm{Ln}|\xi(b)| - \mathrm{Ln}|\xi(a)|).\end{aligned}$$

We propose a simpler variation of this technique inspired in the work by Fettis [39]. It is based in two principles:

- The Cauchy Principal Value consists of e valuating the integral excluding a symmetric and arbitrarily small boundary around the singularity. The singular kernel can be expressed in terms of its series expansion, giving: $f = \frac{a}{r} + b + cx + dx^2 + \cdots$ Using the property that the terms of order $2n-1$ are antimetric, $(r)^{2n-1} = -(-r)^{2n-1}$, we can decompose the integral in two parts and do the specular range of one of them in order to get the antimetric terms, which will vanish. Among these terms, the singular one $\frac{a}{r}$ is one of the vanishing terms

$$\begin{aligned}\int_{-1}^{1} f(x)\,\mathrm{d}x &= \int_{-1}^{-\varepsilon} f(x)\,\mathrm{d}x + \int_{\varepsilon}^{1} f(x)\,\mathrm{d}x \\ &= \int_{\varepsilon}^{1} f(-x)\,\mathrm{d}x + \int_{\varepsilon}^{1} f(x)\,\mathrm{d}x \\ &= \int_{\varepsilon}^{1} (f(x) + f(-x))\,\mathrm{d}x\end{aligned}$$

  the terms involved are

$$\begin{aligned}&\int_{\varepsilon}^{1} (f(x) + f(-x))\,\mathrm{d}x \\ &\quad = \int_{\varepsilon}^{1} \left(\left(\frac{a}{x} + b + cx + dx^2 + \cdots\right)\right. \\ &\qquad \left. + \left(-\frac{a}{x} + b - cx + dx^2 - \cdots\right)\right)\mathrm{d}x \\ &\quad = \int_{\varepsilon}^{1} (2b + 2dx^2 + \cdots)\,\mathrm{d}x\end{aligned}$$

  which is bounded at the singularity and may be written as

$$\begin{aligned}\int_{\varepsilon}^{1} (2b + 2dx^2 + \cdots)\,\mathrm{d}x &= \int_{0}^{1} (2b + 2dx^2 + \cdots)\,\mathrm{d}x \\ &= \int_{0}^{1} (f(x) + f(-x))\,\mathrm{d}x.\end{aligned}$$

- We apply a change of variable in order to center the singularity, transforming any collocation point in natural coordinates into zero. The main property this change needs is to keep the continuity and the derivability over the range, especially at the singularity. The simplest change found is the following:

$$\xi(t) = \mathrm{sign}(\xi_c)\left[1 - (1 - |\xi_c|)(1 - \mathrm{sign}(\xi_c)\xi)\mathrm{e}^{-\mathrm{Ln}\frac{1}{1-|\xi_c|}\mathrm{sign}(\xi_0)t}\right].$$

The process can be schematized in Fig. B.1. Therefore the integral is done as

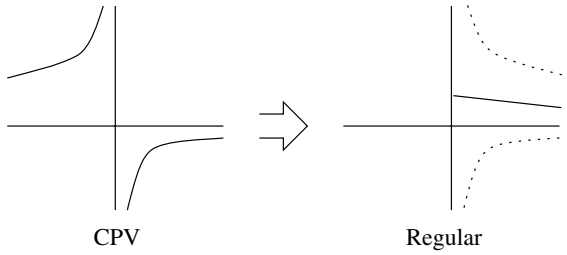

Fig. B.1. Steps in the regularization of 1-singular integrals.

$$I=\int_\Gamma A\,\mathrm{d}\Gamma=\int_{-1}^{1}A(\xi)J(\xi)\,\mathrm{d}\xi=\int_0^1 F(t)-F(-t)\,\mathrm{d}t,$$

where

$$A=\frac{\phi}{r},\quad J=\frac{\mathrm{d}\Gamma}{\mathrm{d}\xi},\quad J_1(t)=\frac{\mathrm{d}\xi}{\mathrm{d}t},$$
$$F(t)=A(\xi(t))J(\xi(t))J_1(t),$$
$$\xi(t)=\mathrm{sign}(\xi_c)\left[1-(1-|\xi_c|)(1-\mathrm{sign}(\xi_c)\xi)\mathrm{e}^{-\mathrm{Ln}\frac{1}{1-|\xi_c|}\mathrm{sign}(\xi_0)t}\right],$$
$$J_1(t)=(1-|\xi_c|)\left(1+\mathrm{Ln}\frac{1}{1-|\xi_c|}(1-\mathrm{sign}(\xi_c)\xi)\right)\mathrm{e}^{-\mathrm{Ln}\frac{1}{1-|\xi_c|}\mathrm{sign}(\xi_0)t}.$$

B.5. $\frac{1}{r^2}$-Singular

Following the method for computation of hypersingular Kernels completely defined by Guiggianni [38], one may use the formulas,

$$I=\lim_{\varepsilon\to0^+}\left\{\int_{\Gamma_s-S_\varepsilon}A(y,x)\,\mathrm{d}\Gamma(x)+\frac{B}{\varepsilon}\right\}$$
$$I=\sum_{m=1}^{2}\left\{\int_{-1}^{1}\left[F^m(\eta,\xi)-\left(\frac{F^m_{-2}(\eta)}{(\xi-\eta)^2}+\frac{F^m_{-1}(\eta)}{\xi-\eta}\right)\right]\mathrm{d}\xi\right.$$
$$+F^m_{-1}(\eta)\ln\left|\frac{2}{\beta_m(\eta)}\right|\mathrm{sign}(\xi-\eta)$$
$$\left.-F^m_{-2}(\eta)\left[\mathrm{sign}(\xi-\eta)\frac{\gamma_m(\eta)}{\beta_m(\eta)^2}+\frac{1}{2}\right]\right\}$$

($\eta=1$ for $m=1$, and $\eta=-1$ for $m=2$) when the singularity is placed between two elements and, in the case of a mid-node collocation point,

$$I=\int_{-1}^{1}\left[F(\eta,\xi)-\left(\frac{F_{-2}(\eta)}{(\xi-\eta)^2}+\frac{F_{-1}(\eta)}{\xi-\eta}\right)\right]\mathrm{d}\xi$$
$$+F_{-1}(\eta)\ln\left|\frac{1-\eta}{-1-\eta}\right|-F^{-2}(\eta)\left[\frac{-1}{1-\eta}+\frac{1}{-1-\eta}\right]$$

($\eta\in(-1,1)$) where y and η are the collocation point in real and local coordinates, and x and ξ are the integration point in real and local coordinates ($-1\leqslant\xi\leqslant1$). The terms β_m and γ_m account for the distortion by the local coordinates transformation of the originally symmetric vicinity of the collocation point

$$F(\eta,\xi)=A(y(\eta),x(\xi))J^m(\xi)=\frac{F_{-2}(\eta)}{(\xi-\eta)^2}+\frac{F_{-1}(\eta)}{\xi-\eta}+\mathrm{O}(1),$$
$$\beta_m=\frac{1}{J^m(\eta)}=\frac{1}{\sqrt{\left(\frac{\partial x_1}{\partial\xi}\right)^2+\left(\frac{\partial x_2}{\partial\xi}\right)^2}},$$
$$\gamma_m=-\frac{\frac{\partial x_1}{\partial\xi}\frac{\partial^2x_1}{\partial\xi^2}+\frac{\partial x_2}{\partial\xi}\frac{\partial^2x_2}{\partial\xi^2}}{2J^m(\eta)^4}=-\frac{\frac{\partial x_1}{\partial\xi}\frac{\partial^2x_1}{\partial\xi^2}+\frac{\partial x_2}{\partial\xi}\frac{\partial^2x_2}{\partial\xi^2}}{2\left\{\left(\frac{\partial x_1}{\partial\xi}\right)^2+\left(\frac{\partial x_2}{\partial\xi}\right)^2\right\}^2}.$$

An alternative method was later proposed by Saez and Gallego [37], and reads in the case of a collocation point inside the element,

$$I=\int_\Gamma\frac{1}{r^2}\left|\frac{\mathrm{d}r(x)}{\mathrm{d}\Gamma}\right|\left[\phi(x)-\phi(x_c)-r\frac{\mathrm{d}\phi(x_c)}{\mathrm{d}r}\right]\mathrm{d}\Gamma$$
$$-\phi(x_c)\left[\frac{1}{R_1}+\frac{1}{R_2}\right]+\frac{\mathrm{d}\phi(x_c)}{\xi}\frac{1}{J(x_c)}\ln\left[\frac{R_2}{R_1}\right],$$

where

$$A(x,y)=\frac{1}{r^2}\phi(x),$$
$$\phi(x)=\phi(x_c)+r\frac{\mathrm{d}\phi(x_c)}{\mathrm{d}r}+\mathrm{O}(r^2),$$
$$\frac{\mathrm{d}\phi(x_c)}{\mathrm{d}r}=\frac{\mathrm{d}\phi(x_c)}{\xi}\frac{1}{J(x_c)}\mathrm{sign}\left(\frac{\mathrm{d}r(x_c)}{\mathrm{d}\Gamma}\right).$$

We propose and use a development from the idea of Fettis [39] that yields the following formula, whose main advantage is that it does not require the calculation of a further derivative of the kernel. The main advantages of the change of variable is that it annihilates the free terms by its symmetry, and moreover it simplifies the integrals to only a regular one without need for a second asymmetric one, as done in [39].

The integral is eventually implemented as

$$I=\int_\Gamma A\,\mathrm{d}\Gamma=\int_{-1}^{1}A(\xi)J(\xi)\,\mathrm{d}\xi$$
$$=\int_0^1\frac{F(t)-F(-t)}{t}\,\mathrm{d}t-\phi(x_c)\left[\frac{1}{r(1)}+\frac{1}{r(-1)}\right],$$

where

$$A=\frac{\phi}{r^2},\quad J=\frac{\mathrm{d}\Gamma}{\mathrm{d}\xi},\quad J_1(t)=\frac{\mathrm{d}\xi}{\mathrm{d}t},$$
$$F(t)=\left(\frac{G(\xi(t))-G_0(\xi(t))\left|\frac{\mathrm{d}r(\xi(t))}{\mathrm{d}\Gamma}\right|}{t}\right)J(\xi(t))J_1(t),$$
$$G(\xi(t))=A(\xi(t))t^2,\quad G_0(\xi(t))=\phi(\xi_c)\frac{t^2}{r^2(\xi(t))},$$
$$\xi(t)=\mathrm{sign}(\xi_c)\left[1-(1-|\xi_c|)(1-\mathrm{sign}(\xi_c)\xi)\mathrm{e}^{-\mathrm{Ln}\frac{1}{1-|\xi_c|}\mathrm{sign}(\xi_0)t}\right],$$
$$J_1(t)=(1-|\xi_c|)(1+\mathrm{Ln}\frac{1}{1-|\xi_c|}(1-\mathrm{sign}(\xi_c)\xi))\mathrm{e}^{-\mathrm{Ln}\frac{1}{1-|\xi_c|}\mathrm{sign}(\xi_0)t},$$
$$\left|\frac{\mathrm{d}r}{\mathrm{d}\Gamma}\right|=\left|\frac{r_1t_1+r_2t_2}{r}\right|.$$

The sign should always be nonzero for any argument.

This formula can be derived in the following way. The basic steps if the regularization itself are shown in Fig. B.2. The Hadamard finite part is defined as an integral in which some infinite term is eliminated,

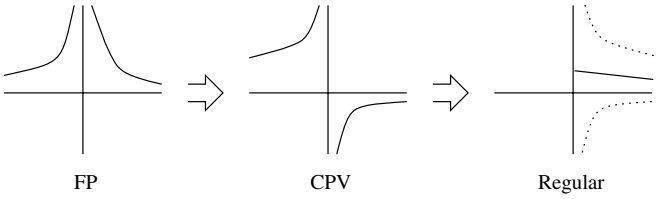

Fig. B.2. Steps for regularization of 2-singular integrals.

$$I = \int_\Gamma^{\mathrm{FP}} A\,\mathrm{d}\Gamma = \int_\Gamma^{\mathrm{FP}} \frac{\phi(s)}{r^2(s)}\,\mathrm{d}\Gamma(s) = \lim_{\varepsilon\to 0}\left[\int_{s_i}^{s_c-\varepsilon} \frac{\phi(s)}{r^2(s)}\,\mathrm{d}\Gamma(s) + \int_{s_c+\varepsilon}^{s_f} \frac{\phi(s)}{r^2(s)}\,\mathrm{d}\Gamma(s) - \phi(s_c)\left(\frac{1}{r(-\varepsilon)} + \frac{1}{r(\varepsilon)}\right)\right].$$

If we develop the kernel with a simplified notation,

$$I = \int_\Gamma^{\mathrm{FP}} A\,\mathrm{d}\Gamma = \int_\Gamma^{\mathrm{FP}} \frac{\frac{\phi t^2}{r^2}}{t^2}\,\mathrm{d}\Gamma = \int_\Gamma^{CPV} \frac{\frac{\phi t^2}{r^2} - \frac{\phi_c t^2}{r^2}\left|\frac{\mathrm{d}r}{\mathrm{d}\Gamma}\right|}{t^2}\,\mathrm{d}\Gamma + \int_\Gamma^{\mathrm{FP}} \frac{\phi_c}{r^2}\left|\frac{\mathrm{d}r}{\mathrm{d}\Gamma}\right|\mathrm{d}\Gamma.$$

Here, $G = \frac{\phi t^2}{r^2}$, doing the symmetric change of variable, doing the same considerations as for the $\frac{1}{r}$ integrals, and defining $F = \frac{\frac{\phi t^2}{r^2} - \frac{\phi_c t^2}{r^2}\left|\frac{\mathrm{d}r}{\mathrm{d}\Gamma}\right|}{t}$,

$$I = \int_{-1}^{1,CPV} \frac{\frac{\phi t^2}{r^2} - \frac{\phi_c t^2}{r^2}\left|\frac{\mathrm{d}r}{\mathrm{d}\Gamma}\right|}{t^2} JJ_1\,\mathrm{d}t + \lim_{\varepsilon\to 0}\phi_c\left[\frac{1}{r(-\varepsilon)^2} - \frac{1}{r(-1)^2} - \frac{1}{r(1)^2} + \frac{1}{r(\varepsilon)^2}\right] - \lim_{\varepsilon\to 0}\phi_c\left[\frac{1}{r(-\varepsilon)^2} + \frac{1}{r(\varepsilon)^2}\right]^{\text{by FP definition}} = \int_0^1 \frac{F(t)-F(-t)}{t}\,\mathrm{d}t - \phi_c\left[\frac{1}{r(-1)^2} + \frac{1}{r(1)^2}\right].$$

Some considerations are useful:

- G is bounded and Hölder continuous.
- F is bounded and Hölder continuous.
- The kernel of the integral $\frac{F(t)-F(-t)}{t}$ is bounded and Hölder continuous, and the range of the integral may be modified from $t(\varepsilon) \to 1$ to $0 \to 1$.

More references about the basics on integration, Krommer [40] and Lutz [41], computation of bessel functions [42,43] and regularization can be found, in order of appearance, in [44,45,39,46–52].

References

[1] S. Kubo, Classification of inverse problems arising in field problems and their treatments, in: M. Tanaka, H.D. Bui (Eds.), Inverse Problems in Engineering Mechanics, Springer Verlag, Tokyo, Japan, 1992, pp. 51–60.
[2] G. Stavroulakis, H. Antes, Unilateral crack identification: a filter-driven interartive, boundary element approach, J. Global Optim. 17 (2000) 339–352.
[3] N. Nishimura, S. Kobayashi, Determination of cracks having arbitrary shapes with the boundary integral equation method, Engrg. Anal. Bound. Elem. 15 (1994) 189–195.
[4] R.A. Meric, Differential and integral sensitivity formulations and shape optimization by BEM, Engrg. Anal. Bound. Elem. 15 (1995) 181–188.
[5] R. Aithal, S. Saigal, Shape sensitivity in thermal problems using BEM, Engrg. Anal. Bound. Elem. 15 (1995) 115–120.
[6] S.C. Mellings, M.H. Aliabadi, Flaw identification using the boundary element method, Int. J. Numer. Methods Engrg. 38 (1995) 399–419.
[7] B.Y. Lee, B.M. Kwak, Shape optimization of two-dimensional thermoelastic structures using boundary integral equation formulation, Comput. Struct. 41 (4) (1991) 709–722.
[8] G. Rus, R. Gallego, Solution of identification inverse problems by a sensitivity boundary integral equation, Barcelona, September 2000, in: E. Oñate, G. Bugeda, B. Suárez (Eds.), ECCOMAS2000, 2000.
[9] S. Mukherjee, X. Shi, Y.X. Mukherjee, Surface variables and their sensitivities in three-dimensional linear elasticity by the boundary contour method, Comput. Methods Appl. Mech. Engrg. 173 (1999) 387–402.
[10] S. Mukherjee, X. Shi, Y.X. Mukherjee, Internal variables and their sensitivities in three-dimensional linear elasticity by the boundary contour method, Comput. Methods Appl. Mech. Engrg. 187 (2000) 289–306.
[11] A.-V. Phan, S. Mukherjee, On design sensitivity analysis in linear elasticity by the boundary contour method, Engrg. Anal. Bound. Elem. 23 (1999) 195–199.
[12] M. Bonnet, Boundary element based formulations for crack shape sensitivity analysis, Engrg. Anal. Bound. Elem. 25 (2001) 347–362.
[13] S.N. Fata, B.B. Guzina, M. Bonnet, Computational basics for elastodynamic cavity identification in a semi-infinite solid, in: S.A. Kinnas (Ed.), International Association for Boundary Element Methods, UT, Austin, TX, USA, 2002.
[14] M. Bonnet, T. Burczyński, M. Nowakowski, Sensitivity analysis for shape perturbation of cavity or internal crack using BIE and adjoint variable approach, Int. J. Solids Struct. 39 (2002) 2365–2385.
[15] T. Burczyński, J.H. Kane, C. Balakrishna, Shape design sensitivity analysis via material derivative-adjoint variable technique for 3-D and 2-D curved boundary elements, Int. J. Numer. Methods Engrg. 38 (1995) 2839–2866.
[16] B. Guzina, S. Fata, M. Bonnet, On the stress-wave imaging of cavities in a semi-infinite solid, Int. J. Solids Struct. 40 (6) (2003) 1505–1523.
[17] M. Tanaka, Y. Masuda, Boundary element method applied to some potential inverse problems, Engrg. Anal. 3–3 (1989) 138–143.
[18] R. Gallego, J. Suárez, Solution of inverse problems by boundary integral equations without residual minimization, Int. J. Solids Struct. 37 (1999) 5629–5652.
[19] G. Rus, R. Gallego, Boundary integral equation for inclusion and cavity shape sensitivity in harmonic elastodynamics, Engrg. Anal. Bound. Elem. 25 (2005) 77–91.
[20] M. Bonnet, Boundary integral equations and material differentiation applied to the formulation of obstacle inverse problems, Engrg. Anal. Bound. Elem. 15 (1995) 121–136.
[21] J. Domínguez, Boundary Elements in Dynamics, Elsevier, CMP, 1993.
[22] M. Guiggiani, Hypersingular formulation for boundary stress evaluation, Engrg. Anal. Bound. Elem. 13 (2) (1994) 169–179.
[23] R. Gallego, J. Domínguez, Hypersingular BEM for transient elastodynamics, Int. J. Numer. Methods Engrg. 39 (1996) 1681–1705.
[24] F. Chirino, R. Abascal, Cálculo de factores de intensidad de tensión estáticos y dinámicos mediante el método de los elementos de contorno con formulación hipersingular, Métodos numéricos para cálculo y diseño en ingeniería 14 (3) (1998) 339–364.

[25] R. Gallego, J. Suárez, Numerical solution of the variation boundary integral equation for inverse problems, Int. J. Numer. Methods Engrg. 49 (1999) 501–518.
[26] M. Bonnet, Differentiability of strongly singular and hypersingular boundary integral formulations with respect to boundary perturbations, Comput. Mech. 19 (1997) 240–246.
[27] M. Altmann, About nonuniform rational b-splines – nurbs, worcester Polytechnic Institute, USA. www.cs.wpi.edu/~matt/cs563/talks/nurbs.html.
[28] G.J. Vass, The bezier curve. a pov-ray tutorial, www.geocities.com/CapeCanaveral/Launchpad/7394/.
[29] L.M. Bezerra, S. Saigal, A boundary element formulation for the inverse elastostatics problem (IESP) of flaw detection, Int. J. Numer. Methods Engrg. 36 (1993) 2189–2202.
[30] Z. Yao, B. Gong, Defect identification using boundary element methods of elastostatics, in: T. e.a. Bui (Ed.), Inverse Problems in Engineering Mechanics, 1994.
[31] M. Prud'homme, T.H. Nguyen, Iterative solution to the inverse steady state convection: analysis of the convergence process., in: E. Oñate, G. Bugeda, B. Suárez (Eds.), ECCOMAS2000, 2000.
[32] J.E. Dennis, Jr., R.B. Schnabel, Numerical Methods for Unconstrained Optimization and Nonlinear Equations, SIAM, Philadelphia, 1983, 1996.
[33] L. Rsde, B. Westergren, Mathematics Handbook for Science and Engineering, Springer, 1999.
[34] M. Inc., Matlab optimization toolbox user's guide, http://www.mathworks.com (1996).
[35] G. Rus, R. Gallego, Optimization algorithms for identification inverse problems with the boundary element method, Engrg. Anal. Bound. Elem. 26 (2002) 315–327.
[36] G. Rus, R. Gallego, Optimization algorithms for identification inverse problems, in: E. Oñate, G. Bugeda, B. Suárez (Eds.), CMEM2001, 2001.
[37] A. Sáez, R. Gallego, J. Domínguez, Hypersingular quarter-point boundary elements for crack problems, Int. J. Numer. Methods Engrg. 38 (1995) 1681–1701.
[38] M. Guiggiani, Direct evaluation of hypersingular integrals in 2D BEM, in: W.H. Vieweg (Ed.), Proc. 7th GAMM Seminar on Numerical Techniques for Boundary Element Methods/Notes in Numerical Fluid Mechanics, vol. 333, Kiel, Germany, 1991, pp. 23–34.
[39] H.E. Fettis, Expressions for divergent integrals in terms of convergent ones, in: G. Hammerlin (Ed.), Numerical Integration International Series of Numerical Mathematics, Birkhauser, 1991.
[40] A.R. Krommer, C.W. Ueberhuber, Computational Integration, SIAM, 1998.
[41] E.D. Lutz, Numerical methods for hypersingular and near-singular boundary integrals in fracture mechanics, Ph.D. thesis, Cornell University, Ithaca, New York, USA, 1991.
[42] I.S. Gradshteyn, I.M. Ryzhik, Table of Integral, Series, and Products, Academic Press, 1963.
[43] M. Abramowitz, I.A. Stegun, Handbook of Mathematical Functions, Dover, 1964.
[44] L. Jun, G. Beer, J.L. Meek, Efficient evaluation of integrals of order $1/r$, $1/r^2$, $1/r^3$, using Gauss method, Engng. Anal. 2 (1985) 118–123.
[45] J.C.F. Telles, A self-adaptative coordinate transformation for efficient numerical evaluation of general boundary element integrals, Int. J. Numer. Methods Engrg. 24 (1987) 959–973.
[46] M. Guiggiani, G. Krishnasamy, F.J. Rizzo, T.J. Rudolphi, Hypersingular boundary integral equations: a new approach to their numerical treatment, in: L. Morino, R.P. . Springer (Eds.), Proc. IABEM Symposium/Boundary Integral Methods, Rome, Italy/Berlin, Germany, 1990, pp. 211–220.
[47] M. Guiggiani, G. Krishnasamy, T.J. Rudolphi, F.J. Rizzo, A general algorithm for the numerical solution of hypersingular boundary integral equations, J. Appl. Mech. 59 (1992) 604–614.
[48] T. Rudolphi, The use of simple solutions in the regularization of hypersingular boundary integral equations, Math. Comput. Modell. 15 (3-5) (1991) 269–278.
[49] V. Saldek, J. Sladek, M. Tanaka, Regularization of hypersingular and nearly singular integrals in the potential theory and elasticity, Int. J. Numer. Methods Engrg. 36 (1993) 1609–1628.
[50] Q. Huang, T. Cruse, Some notes on singular integral techniques in boundary element analysis, Int. J. Numer. Methods Engrg. 36 (1993) 2643–2659.
[51] N.A. Dumont, On the efficient numerical evaluation of integrals with complex singularity poles, Engrg. Anal. Bound. Elem. 13 (1994) 155–168.
[52] M. Tanaka, V. Sladek, J. Sladek, Regularization techniques applied to boundary element methods, Appl. Mech. Rev. 47 (10) (1994) 457–499.